

Differential reorganization of three syntax-related networks induced by a left frontal glioma

Ryuta Kinno,^{1,2,3} Shinri Ohta,^{4,5} Yoshihiro Muragaki,^{3,6} Takashi Maruyama^{3,6} and Kuniyoshi L. Sakai^{1,3,4}

1 Department of Basic Science, Graduate School of Arts and Sciences, The University of Tokyo, Tokyo 153-8902, Japan

2 Division of Neurology, Department of Internal Medicine, Showa University Northern Yokohama Hospital, Kanagawa 224-8503, Japan

3 CREST, Japan Science and Technology Agency, Tokyo 102-0075, Japan

4 Department of Life Sciences, Graduate School of Arts and Sciences, The University of Tokyo, Tokyo 153-8902, Japan

5 Japan Society for the Promotion of Science, Tokyo 102-8472, Japan

6 Department of Neurosurgery, Tokyo Women's Medical University, Tokyo 162-8666, Japan

Correspondence to: Kuniyoshi L. Sakai
Department of Basic Science,
Graduate School of Arts and Sciences,
The University of Tokyo,
3-8-1 Komaba, Meguro-ku,
Tokyo 153-8902, Japan
E-mail: sakai@mind.c.u-tokyo.ac.jp

The opercular/triangular parts of the left inferior frontal gyrus and the left lateral premotor cortex are critical in syntactic processing. We have recently indicated that a glioma in one of these regions is sufficient to cause agrammatic comprehension. In the present study, we aimed to show how normally existing syntax-related networks are functionally reorganized by a lesion. Twenty-one patients with a left frontal glioma preoperatively performed a picture–sentence matching task, and underwent functional magnetic resonance imaging scans in an event-related design. We established two qualitatively different types of agrammatic comprehension, depending on glioma location. Patients with a glioma in the left lateral premotor cortex had a more profound deficit in the comprehension of scrambled sentences than that of active and passive sentences. In contrast, patients with a glioma in the opercular/triangular parts of the left inferior frontal gyrus had a more profound deficit in the comprehension of passive and scrambled sentences than that of active sentences. Moreover, we found dramatic changes in the activation patterns in these two patient groups, which accompanied abnormal overactivity and/or underactivity in the syntax-related regions. Furthermore, by examining functional connectivity in the normal brain, we identified three syntax-related networks among those regions, and anatomically visualized connections within individual networks by using diffusion tensor imaging. The first network consists of the opercular/triangular parts of the left inferior frontal gyrus, left intraparietal sulcus, right frontal regions, presupplementary motor area, and right temporal regions. These regions were overactivated in the patients with a glioma in the left lateral premotor cortex only for correct responses, indicating a cognitive change. The second network consists of the left lateral premotor cortex, left angular gyrus, lingual gyrus, and cerebellar nuclei. These regions were overactivated in the patients with a glioma in the opercular/triangular parts of the left inferior frontal gyrus for both correct and incorrect responses, indicating a neuronal change. The third network consists of the left ventral frontal and posterior temporal regions. These regions were underactivated in the patients with a glioma in the opercular/triangular parts of the left inferior frontal gyrus, indicating another neuronal change. These results demonstrate that agrammatic comprehension is associated with the global reorganization of functionally distinct networks, which indeed reflects a differential change in the relative contribution of these three networks to normal syntax-related functions.

Keywords: agrammatism; language; glioma; frontal cortex; MRI

Abbreviations: F3 = inferior frontal gyrus; LPMC = lateral premotor cortex

Introduction

Cortical reorganization is one of the fundamental issues in clinical neuroscience. For example, homotopic reorganization, i.e. activation in a contralesional homologous region, is induced by acute lesions after stroke (Saur *et al.*, 2006) or by slow-growing lesions such as gliomas (Desmurget *et al.*, 2007), as observed by functional MRI. However, homotopic reorganization occurs only in a subset of patients, and its exact neural mechanisms remain unknown. Although neurovascular uncoupling (Ulmer *et al.*, 2004) or an abnormality of transcallosal inhibition leading to disinhibition (Thiel *et al.*, 2006) has been considered to explain such reorganization, these theories are still not conclusive. Therefore, differential activation patterns between patients and normal participants should be thoroughly examined by using functional and anatomical imaging techniques. Abnormal activity in patients is indicated by overactivity (or underactivity), in which a given region is recruited more (or less) than normal during a cognitive task, and such an abnormality reflects cognitive and/or neuronal changes. Although neuronal changes are mediated by changes in the strength of pre-existing connections, cognitive changes occur when a patient uses a different set of cognitive processes, either because of increased demands on normal processes, or because a new cognitive procedure has been learned (Price and Friston, 1999). In the present study with agrammatic patients, we focused on the fundamental syntactic processes. We aimed to show how normally existing syntax-related networks are functionally reorganized by a lesion.

Previous functional neuroimaging studies of normal participants have already established that the opercular/triangular parts of the left inferior frontal gyrus (F3), as well as the left lateral premotor cortex (LPMC), play a crucial role in syntactic processes (Stromswold *et al.*, 1996; Dapretto and Bookheimer, 1999; Embick *et al.*, 2000; Hashimoto and Sakai, 2002; Sakai *et al.*, 2002; Friederici *et al.*, 2003; Musso *et al.*, 2003; Suzuki and Sakai, 2003); these regions have been proposed as putative grammar centres (Sakai, 2005). Moreover, we clarified that these two regions are differentially modulated during syntactic processing (Kinno *et al.*, 2008). For patients with a left frontal glioma, we have recently indicated that a glioma in one of these regions is sufficient to cause agrammatic comprehension (Kinno *et al.*, 2009). In the present functional MRI study, we analysed activation patterns of agrammatic patients with a left frontal glioma to identify any cortical reorganization of syntax-related networks.

We predict that there are multiple syntax-related networks, each of which partially includes lateral sides of frontal, temporal, and parietal regions, as well as medial regions and cerebellum. These candidate regions have been already indicated by our previous functional MRI studies (Suzuki and Sakai, 2003; Kinno *et al.*, 2008). We further hypothesize that there exist at least three syntax-related networks, corresponding to three regions of the left LPMC, opercular/triangular parts of the left F3, and

triangular/orbital parts of the left F3, which were identified to have distinct functional roles during sentence comprehension (Sakai, 2005). By using functional MRI data in the present study, functional connectivity among activated regions was assessed to reveal these three sets of functionally correlated regions during a syntactic task. We used all time-series data from the normal participants alone, as abnormal brains might reflect coincidental co-activation or co-deactivation.

The recent diffusion tensor imaging studies have suggested two different pathways for language processing in the normal or abnormal brain: the dorsal tracts of the arcuate and superior longitudinal fasciculi, and ventral tracts of the middle longitudinal fasciculus and extreme capsule (Saur *et al.*, 2008; Rolheiser *et al.*, 2011; Wilson *et al.*, 2011; Wong *et al.*, 2011). The dorsal pathways may be further divided into two: one connecting the LPMC and temporal gyrus for sensory to motor mapping, the other connecting the F3 and temporal gyrus for semantic and syntactic functions in sentence comprehension (Friederici, 2011). However, the relative contributions of these pathways to syntactic processing and related functions, as well as their functional divisions within the syntax-related networks, remain unclear. As a substantial amount of white matter is usually included in each patient's tumour (see the grey matter ratio in Table 1), any fibres originated from the focal lesion may also have been partially defective. Therefore, to provide empirical backup for the networks deduced from the activation studies of the normal participants, we referred to normal data of fibre tracking. Our current results will clarify the principles of global reorganization within the syntax-related networks induced by focal lesions.

Materials and methods

Here, we provided an overview of the experimental conditions and procedures used to acquire the data presented; full details are provided in the Supplementary material.

Participants

We tested 21 patients, who were native Japanese speakers newly diagnosed as having a left frontal glioma (Table 1). The patients pre-operatively performed a picture–sentence matching task (Fig. 1A), and underwent functional MRI scans in an event-related design. The patients were divided into three groups based on the individual tumour locations in the normalized brain (Fig. 1B): patients with a glioma in the left LPMC (LPMC group, $n = 7$); patients with a glioma in the opercular/triangular parts of the left F3 (F3 group, $n = 7$); and patients with a glioma in the other left frontal regions (Other group, $n = 7$). The categorization criterion of each group was whether or not the glioma of a patient overlapped, at least partially on a voxel-by-voxel basis, with functionally identified regions in our previous study (Kinno *et al.*, 2008): the left LPMC and opercular/triangular parts of the left F3 shown in Figs 3 and 4 in Kinno *et al.* (2008), respectively.

Table 1 Patient demographics

Patient	Gender	Age	Laterality quotient	Verbal/non-verbal IQ	Hemispheric dominance	Tumour location	Tumour volume (mm ³)	Grey matter ratio	Tumour type	Tumour grade
LPMC group										
Patient 1	M	31	88	102/92	Left	L. F1/F2/SMA/LPMC	40096	57.3	AO	III
Patient 2 ^a	M	47	81	105/102	Left	L. F1/F2/SMA/LPMC/F3op	33214	56.3	AOA	III
Patient 3 ^a	M	36	88	102/92	Left	L. F1/F2/SMA/LPMC/F3op	89137	59.8	AA	III
Patient 4	M	49	100	98/96	Left	L. F1/F2/LPMC	30148	58.0	AO	III
Patient 5	F	34	100	99/90	Left	L. F1/F2/LPMC/F3op	29375	52.6	OD	II
Patient 6	M	29	81	106/102	Left	L. F1/F2/LPMC/F3op	38003	50.5	AO	III
Patient 7 ^a	F	27	45	101/95	Left	L. F2/LPMC/F3op	22393	56.9	DA	II
Mean ± SD		36 ± 8.6	83 ± 19	102 ± 3.0/96 ± 4.8		40338 ± 22300		56 ± 3.2		
F3 group										
Patient 8	M	32	54	101/98	Left	L. F1/F2/F3op/F3O/insula	25471	59.0	AOA	III
Patient 9	F	20	100	98/101	Left	L. F1/F2/F3op/F3O/insula	74556	52.2	AO	III
Patient 10	M	31	100	99/100	Left	L. F1/F2/F3op/F3t/insula/striatum	53297	58.1	AOA	III
Patient 11	M	32	100	95/109	Left	L. F1/F2/F3op/F3O/insula/striatum	57650	56.3	DA	II
Patient 12 ^a	F	42	90	95/109	Left	L. F2/F3op/F3O/insula/striatum	74543	59.8	OA	II
Patient 13	F	29	87	91/93	Left	L. F2/F3op/F3O/insula/striatum	36863	50.9	OD	II
Patient 14 ^a	M	47	73	93/100	Left	L. F3op/F3t/insula/striatum	18120	54.3	DA	II
Mean ± SD		33 ± 8.8	86 ± 17	96 ± 3.5/101 ± 5.8		48643 ± 22555		56 ± 3.4		
Other group										
Patient 15 ^a	F	62	89	98/101	Left	L. F1/F2/SMA	49301	55.3	AO	III
Patient 16	M	24	68	94/98	Left	L. F1/F2/SMA/striatum	63795	58.0	OA	II
Patient 17	F	38	100	106/113	Left	L. F1/F2/SMA/striatum	51081	54.7	AOA	III
Patient 18	F	21	100	106/106	Left	L. F1/F2/F3t/striatum	63051	52.6	DA	II
Patient 19 ^a	F	29	100	86/88	Left	L. F1/F2/F3O/striatum	48932	50.1	AO	III
Patient 20	M	25	100	104/101	Left	L. F1/F2/F3t	14665	53.7	DA	II
Patient 21	M	36	100	90/99	Left	L. F2/F3O	12158	56.7	OA	II
Mean ± SD		34 ± 14	83 ± 12	98 ± 8.0/101 ± 7.6		43283 ± 21323		54 ± 2.6		

^aSeven patients were from our previous study (Kinno *et al.*, 2009). The laterality quotient of handedness was determined by the Edinburgh handedness inventory (Oldfield, 1971). Magnetic resonance images were normalized with SPM8 to determine the tumour location and volume (mm³), as well as the grey matter ratio (%) of a tumour including the grey matter and white matter. The determination of tumour types and grades (II or III, with III being more severe) was based on the World Health Organization Classification of Tumours of the Nervous System (2000). AA = anaplastic astrocytoma (grade III); AO = anaplastic oligodendroglioma (grade III); AOA = anaplastic oligoastrocytoma (grade III); F = female; F1 = superior frontal gyrus; F2 = middle frontal gyrus; F3O = orbital part of the F3; F3op = opercular part of the F3; F3t = triangular part of the F3; IQ = intelligence quotient; L = left; M = male; OA = oligoastrocytoma (grade II); OD = oligodendroglioma (grade II); SD = standard deviation; SMA = supplementary motor area.

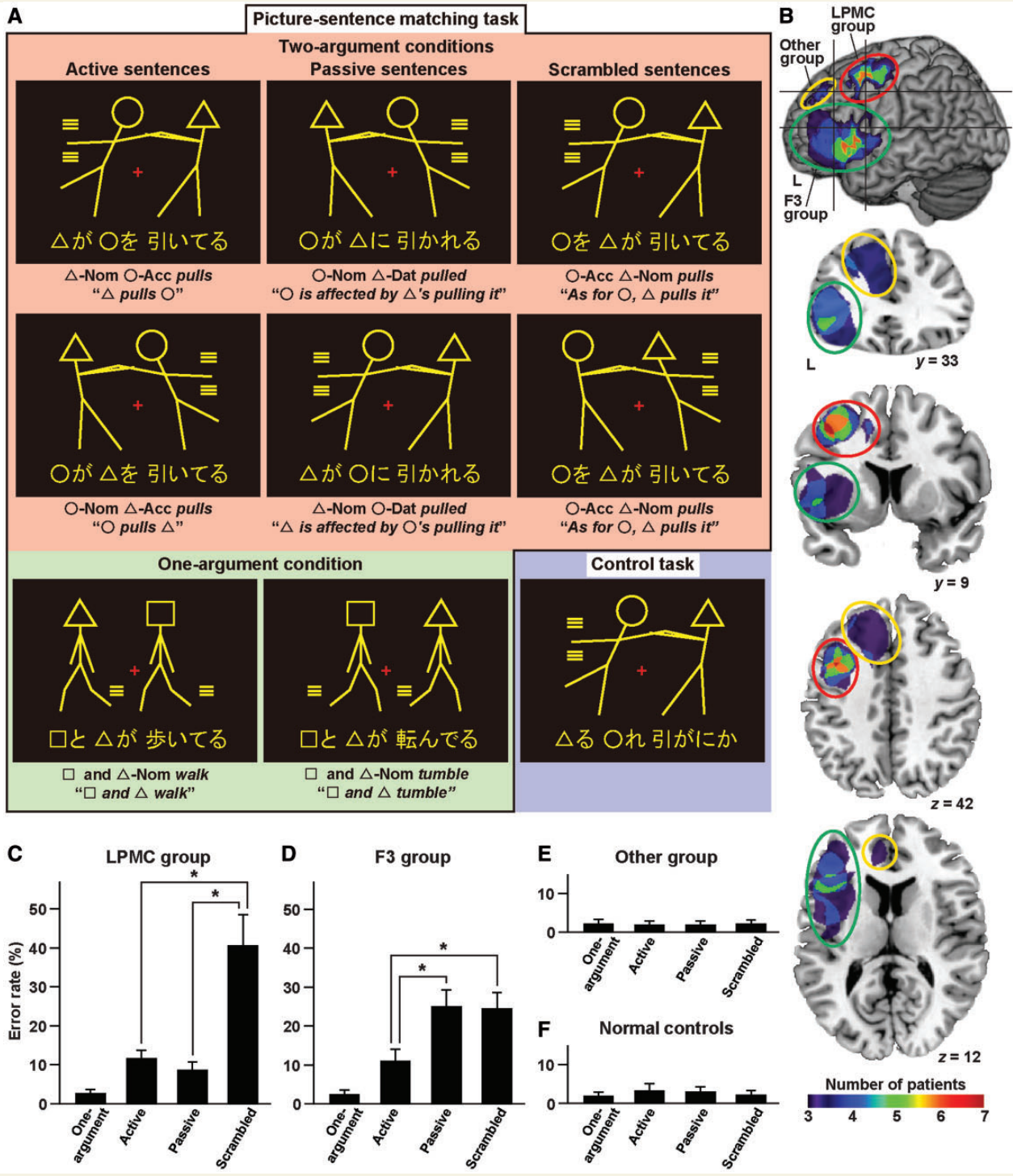


Figure 1 Syntactic task, glioma locations, and agrammatic comprehension. (A) A picture–sentence matching task under either two-argument conditions or one-argument condition; each stimulus consisted of one picture (*top*) and one sentence (*bottom*). Pictures consisted of two stick figures, each of which was distinguished by a ‘head’ symbol: a circle, square or triangle. We used four kinds of grammatical particles, which represent the syntactic information in Japanese: *-ga*, a nominative case marker; *-ni*, a dative case marker; *-o*, an accusative case marker; and *-to*, a coordinator (*and*). Under the two-argument conditions (marked in red), we tested three sentence types: active sentences (e.g. ‘△-*ga* ○-*o* *hiiteru*’ and ‘○-*ga* △-*o* *hiiteru*’), passive sentences (e.g. ‘○-*ga* △-*ni* *hikareru*’ and ‘△-*ga* ○-*ni* *hikareru*’), and scrambled sentences (e.g. ‘○-*o* △-*ga* *hiiteru*’). Examples of matched and mismatched sentences are shown in the first and second rows, respectively. Under the one-argument condition (marked in green), we presented simpler sentences (e.g. ‘□-*to* △-*ga* *aruite*’ and ‘□-*to* △-*ga* *koronderu*’). Examples of matched and mismatched sentences are shown in the *left* and *middle* panels of the third row, respectively. For a control task (marked in blue), a matched example is shown in the right panel of the third row. (B) Lesion overlap maps for patient groups. For each group, the full extent of gliomas was overlaid and circled with coloured lines: LPMC group (red),

(continued)

The patients reported here underwent surgery at the Department of Neurosurgery, Tokyo Women's Medical University, after behavioural and functional MRI assessment at the University of Tokyo, Komaba. The following conditions comprised the criteria for inclusion of 21 patients in the present study (Table 1): (i) right-handedness; (ii) no deficits in verbal/written communication or other cognitive abilities reported by the patients or physicians; (iii) no history of neurological or psychiatric disorders other than glioma and seizures; (iv) freedom from seizures with or without antiepileptic drugs; (v) no medical problems related to MRI acquisition; and (vi) completion of at least three functional MRI runs without significant head movement. The laterality quotient of handedness was determined by the Edinburgh handedness inventory (Oldfield, 1971).

In the present study, we recruited seven normal age-matched participants for functional MRI experiments [normal group; five males and two females, aged 25–43 years, 31 ± 5.9 (mean \pm standard deviation)]. Eleven normal age-matched participants (10 males and one female, aged 19–40 years, 29 ± 6.0) were also tested in the diffusion tensor imaging studies. Written informed consent was obtained from each participant after the nature and possible consequences of the studies were explained. Approval for the experiments was obtained from the institutional review board of the University of Tokyo, Komaba, as well as of the Tokyo Women's Medical University.

Lesion analyses

The glioma was first identified on the normalized T_1 -weighted structural image, and the glioma boundary was semi-automatically determined using the 3D Fill tool in MRICroN software, which generated a contiguous cluster of voxels defined by the intensity of the glioma itself. The boundary of each lesion, including brain oedemas and abnormalities of perfusion, was confirmed with T_2 -weighted magnetic resonance images taken at the Department of Neurosurgery, Tokyo Women's Medical University. The absence of any skip lesions distant from a tumour was confirmed with ^{11}C -methionine, ^{18}F -fluorodeoxyglucose, and ^{11}C -choline PET data (resolution = $4.8 \times 4.8 \times 4.25 \text{ mm}^3$) taken at the Chubu Medical Centre for Prolonged Traumatic Brain Dysfunction (Minokamo City, Gifu, Japan).

Stimuli

Each visual stimulus consisted of a picture with head symbols (circle, square or triangle) at the top, and of an always grammatical sentence at the bottom (Fig. 1A). For each stimulus, we chose two different head symbols. The sentences describing actions were written using a combination of the hiragana and kanji writing systems. Using the same task, we tested two types of conditions with different sets of stimuli: two-argument and one-argument conditions. Under the two-argument conditions with an identical picture set, we tested three different sentence types: active, passive, and scrambled sentences. Scrambled sentences are perfectly normal.

Under the two-argument conditions, each sentence ended with a transitive verb, and had two arguments (phrases associated with the predicate) with different grammatical relations (subject, direct object or indirect object) and semantic roles (agent, experiencer or patient). More specifically, the active, passive, and scrambled sentences corresponded to 'subject and direct object' (agent and patient), 'subject and indirect object' (experiencer and agent), and 'direct object and subject' (patient and agent) types, respectively.

Under the one-argument condition, each sentence ended with an intransitive verb, and corresponded to a 'double subjects' (double agents) type, which did not involve two-argument relationships. A linguistically meaningful contrast is thus 'Two-argument – One-argument', where we averaged together activations under the active, passive, and scrambled sentence conditions. This contrast mainly involved syntactic processes, together with minimal semantic processes of semantic role assignment (experiencer/patient) and lexico-semantics (verb types), whereas general cognitive processes were well controlled. All stimuli were presented visually in yellow against a dark background (Fig. 1A). Each stimulus was presented for 5800 ms (intratrial interval) followed by a 200 ms blank interval.

Task

In the picture–sentence matching task, the participants read a sentence covertly and judged whether or not the action depicted in a picture matched the meaning of the sentence. They responded by pressing one of two buttons in a row. Using the same stimulus sets of pictures and letters presented under both two-argument and one-argument conditions, we tested a control task, in which the participants judged whether or not two head symbols in the picture matched those at the bottom, irrespective of their order (Fig. 1A). The letters in hiragana were jumbled without changing the head symbols and kanji, so that the letter string prevented even basic word recognition. General cognitive factors such as visual perception of the stimuli, matching, response selection, and motor responses were controlled by the control task, and by the one-argument condition.

A single run of the task sessions (306 s) contained 24 'test events' of the picture–sentence matching task (six times each under the active, passive, and scrambled sentence conditions, as well as under the one-argument condition), with variable intertrial intervals of one (6 s) or two (12 s) control tasks. The order of the test events was pseudorandomized without repetition of the same condition to prevent any condition-specific strategy. Eight runs were tested per participant in a day.

Magnetic resonance imaging

Data acquisition

The functional MRI scans were conducted on a 1.5 T scanner (Stratis II, Premium; Hitachi Medical Corporation), using a gradient-echo echo-planar imaging sequence (repetition time = 3 s, echo

Figure 1 Continued

F3 group (green), and Other group (yellow). A left lateral surface (horizontal cross hairs at $z = 42$ and 12 ; vertical cross hairs at $y = 33$ and 9) of a standard brain is shown, together with its coronal and axial slices at cross hairs. The colour scale denotes the number of patients ($n \geq 3$). (C–F) Histograms for the error rates of the LPMC group (C), F3 group (D), Other group (E), and normal control subjects (F). Note that the performances for both the LPMC and F3 groups were significantly impaired under the two-argument conditions, but not under the one-argument condition. Error bars indicate the standard error of the mean for the participants, and asterisks denote the significant differences among the two-argument conditions (corrected $P < 0.05$). Acc = accusative case; Dat = dative case; L = left; Nom = nominative case.

time = 50.5 ms, flip angle = 90°, field of view = 192 × 192 mm², resolution = 3 × 3 mm²). The diffusion tensor imaging scans were conducted on a 3.0 T scanner equipped with an 8-channel phased-array head coil (Signa HDxt; GE Healthcare), using a diffusion-weighted spin-echo echo-planar imaging sequence (b -value = 1000 s/mm², repetition time = 15 s, echo time = 86.6 ms, field of view = 256 × 256 mm², resolution = 2 × 2 mm², number of excitations = 2). A single image without diffusion-weighting (b_0) was initially acquired, and then diffusion-weighting was isotropically distributed along 60 diffusion-encoding gradient directions.

Data analyses

Both group and single-subject analyses were performed in a standard manner using SPM8 statistical parametric mapping software (Wellcome Trust Centre for Neuroimaging). To discount any general effects associated with performance differences among the participants, individual error rates averaged among the two-argument conditions, or those of the one-argument condition for the One-argument – Control contrast, were entered as a nuisance factor in a second-level analysis. The results of paired t -tests for the Two-argument – Control, One-argument – Control, and Two-argument – One-argument contrasts were thresholded at $P < 0.005$ for the voxel level, and at corrected $P < 0.05$ for the cluster level, with topological false discovery rate correction across the whole brain, whereas the results of an analysis of covariance with F -test were thresholded at $P < 0.005$ for the voxel level, and at corrected $P < 0.05$ for the cluster level, with family-wise error correction across the whole brain.

By using functional MRI data, functional connectivity among multiple regions was assessed by a partial correlation method for the time-series data of the normal group. From each of the time-series of two regions in question, we regressed out all the other nodes, before estimating the correlation between the two. Data analyses of diffusion tensor imaging were performed using FSL [Oxford Centre for Functional MRI of the Brain's (FMRIB) Software Library 4.1.7] and FDT (FMRIB's Diffusion Toolbox 2.0). To find the connections between two regions of interest, we set two seed masks and retained only those tracts that passed through both seed masks.

Results

Demographics of the patient groups

We characterized the three patient groups to examine whether there were any quantitative or qualitative differences among them (Table 1). The patients' verbal and non-verbal intelligence quotients (both ranges, 86–113 for all patients) were within one standard deviation (± 15) of the mean. According to ANOVA with a factor of group (LPMC, F3, Other), there were no significant differences among the groups in age, laterality quotient of handedness, verbal/non-verbal intelligence quotients, tumour volume or grey matter ratio ($P > 0.1$). Moreover, the error rates under each two-argument condition could not be attributed to these factors, according to the correlation analyses among all patients ($P > 0.1$). Each patient group included two patients without anti-epileptic drug treatment. There are three types of grade II and III gliomas: astrocytic tumours (i.e. diffuse and anaplastic astrocytoma), oligodendroglial tumours (i.e. oligodendroglioma and anaplastic oligodendroglioma), and mixed-type gliomas

(Behin *et al.*, 2003). There were two patients with astrocytic tumours in each patient group. As regards tumour grades, grade II gliomas grow slowly at a constant and continuous rate of ~ 4 mm (in diameter) per year (Mandonnet *et al.*, 2003). Moreover, grade II gliomas systematically change into grade III gliomas (i.e. they undergo anaplastic transformation) within a median of 7–8 years (Duffau, 2005). In the present study, the LPMC group included fewer patients with grade II gliomas, as well as fewer females, than the F3 and Other groups; these two factors are re-examined after the behavioural and activation data are presented.

Agrammatic comprehension caused by a left frontal glioma

According to previous lesion studies (Schwartz *et al.*, 1980; Caplan *et al.*, 1985; Goodglass and Menn, 1985; Menn and Obler, 1990; Pulvermüller, 1995; Grodzinsky, 2000; Kinno *et al.*, 2009), agrammatic patients show relatively good comprehension of single words and simple sentences, but have trouble understanding sentences with more complex syntactic structures. In the present study, we set a two-level criterion as follows. The first-level criterion is an impaired comprehension under the two-argument conditions when compared with the normal participants, in spite of a normal comprehension under the simpler one-argument condition. This criterion precludes any general disorders as a result of visual/motor impairments, attentional disturbances (drowsiness or dizziness) or perseveration for particular responses. In both functional MRI and lesion studies, we have previously indicated that the passive and scrambled sentences required more syntactic analyses for the two-argument relationships than the active sentences that were canonical (Kinno *et al.*, 2008, 2009). The second-level criterion is the higher error rates under the passive and/or scrambled than the active sentence conditions, clearly indicating a syntactic problem, i.e. agrammatic comprehension.

To improve the statistical power of behavioural data, we added 21 normal participants, taken from our previous study with the same experimental protocol (Kinno *et al.*, 2009), to the normal group (normal control subjects; total $n = 28$). The behavioural data of error rates and reaction times are shown in Table 2. Figure 1C–F shows the error rates for each group, which exhibited marked differences among the patient groups. Under each of the two-argument conditions, an ANOVA with a factor of group (LPMC, F3, Other, normal control subjects) showed that there was a clear difference among the groups [active: $F(3,48) = 9.7$, $P < 0.0001$; passive: $F(3,48) = 33$, $P < 0.0001$; scrambled: $F(3,48) = 41$, $P < 0.0001$]. Under all of these two-argument conditions, a Dunnett test showed significantly higher error rates in both the LPMC and F3 groups than the normal control subjects (corrected $P < 0.05$), whereas there was no significant difference between the Other group and normal control subjects (corrected $P > 0.6$). Under the one-argument condition, in contrast, there was no significant difference among the groups [$F(3,48) = 0.40$, $P = 0.76$], confirming that the basic comprehension of sentences required by the one-argument condition was preserved among all of the patients. These results clearly indicate that both the LPMC and F3 groups had trouble understanding sentences with the

Table 2 Behavioural data under each condition

Participant	Error rates (%)					Reaction times (ms)				
	Active sentence	Passive sentence	Scrambled sentence	One-argument	Control	Active sentence	Passive sentence	Scrambled sentence	One-argument	Control
Normal control subjects (<i>n</i> = 28)										
Mean ± SD	3.1 ± 4.1	2.9 ± 3.1	2.2 ± 2.6	1.8 ± 2.0	2.2 ± 1.2	3052 ± 684	3129 ± 642	3242 ± 576	2644 ± 555	2766 ± 426
LPMC group										
Patient 1	16.7	6.3	27.1	0.0	1.9	3385	3218	3397	3212	2869
Patient 2	12.5	12.5	66.7	6.3	0.9	3898	4004	3948	2945	2923
Patient 3	16.7	6.3	54.2	6.3	2.8	3470	3479	3770	2958	3178
Patient 4	8.3	6.3	16.7	0.0	4.6	3105	3259	2908	2667	2676
Patient 5	14.6	16.7	31.3	2.1	2.3	2821	2880	2793	2486	2312
Patient 6	12.5	12.5	66.7	2.1	2.8	3255	3391	3180	2607	3021
Patient 7	0.0	0.0	20.8	2.1	2.8	4184	4286	4249	2739	2662
Mean ± SD	11.6 ± 5.9	8.7 ± 5.6	40.5 ± 21.5	2.7 ± 2.6	2.6 ± 1.1	3445 ± 465	3502 ± 484	3464 ± 546	2802 ± 249	2806 ± 284
F3 group										
Patient 8	12.5	27.1	27.1	2.1	0.5	3673	3720	3742	3214	2406
Patient 9	8.3	27.1	39.6	0.0	3.2	2908	3363	2995	2772	3190
Patient 10	12.5	39.6	31.3	0.0	2.8	3211	3594	3301	2846	2262
Patient 11	8.3	16.7	16.7	4.2	1.4	3350	3242	3103	2712	2414
Patient 12	8.3	16.7	16.7	4.2	2.3	3325	2777	3387	2925	3095
Patient 13	27.1	39.6	31.3	2.1	3.7	3512	3327	3757	1831	2764
Patient 14	0.0	8.3	8.3	4.2	2.3	3783	3850	3915	2895	2867
Mean ± SD	11.0 ± 8.2	25.0 ± 11.9	24.4 ± 10.9	2.4 ± 1.9	2.3 ± 1.2	3395 ± 294	3410 ± 356	3457 ± 353	2742 ± 433	2714 ± 362
Other group										
Patient 15	8.3	6.3	6.3	6.3	0	3867	3949	4385	2959	2833
Patient 16	2.1	4.2	2.1	4.2	2.3	3322	2925	3524	2509	2890
Patient 17	0.0	0.0	0.0	0.0	1.9	2306	2816	2854	2754	2403
Patient 18	2.1	2.1	6.3	4.2	2.3	3148	3106	3165	2407	3179
Patient 19	0.0	0.0	0.0	0.0	4.6	3067	3949	3985	2959	2463
Patient 20	0.0	0.0	0.0	0.0	1.4	3185	2621	3453	2737	2600
Patient 21	0.0	0.0	0.0	0.0	1.9	3237	3632	3674	2818	2871
Mean ± SD	1.8 ± 3.0	1.8 ± 2.6	2.1 ± 3.0	2.1 ± 2.7	2.1 ± 1.4	3161 ± 460	3285 ± 551	3577 ± 507	2735 ± 211	2748 ± 274

Error rates represent per cent incorrect responses per individual per condition; the accuracy is 100 – error rates (%). Reaction times were obtained for correct trials only. SD = standard deviation.

two-argument relationships, thus satisfying the first-level criterion. Moreover, a direct comparison of these two groups with a *t*-test clarified that the F3 group showed significantly higher error rates than the LPMC group under the passive sentence condition [$t(12) = 3.3$, $P = 0.0064$]. This result demonstrates that the deficits of the LPMC group were qualitatively different from those of the F3 group. As regards reaction times, there was no significant difference among the groups under each of the two-argument conditions, as well as under the one-argument condition (ANOVA, $P > 0.3$).

For the second-level criterion, separate comparisons of error rates among the two-argument conditions were performed in individual groups. According to a repeated measures ANOVA with a factor of condition (active, passive, scrambled), there was a significant difference in error rates among the conditions in the LPMC group [$F(2,12) = 16$, $P = 0.0004$] and F3 group [$F(2,12) = 14$, $P = 0.0006$], but not in the Other group [$F(2,12) = 0.16$, $P = 0.86$] or in the normal control subjects [$F(2,54) = 1.6$, $P = 0.21$]. In the LPMC group, the error rates were significantly higher under the scrambled than the active and passive sentence conditions (Bonferroni/Dunn test, corrected $P < 0.05$) (Fig. 1C). In the F3 group, the error rates were

significantly higher under the passive and scrambled than the active sentence conditions (corrected $P < 0.05$) (Fig. 1D). These results satisfy the second-level criterion, and thus the patients in the LPMC and F3 groups had agrammatic comprehension. The normal error rates in the Other group (Fig. 1E) indicate that general medical conditions, including the effect of antiepileptic drug, did not affect patients' performances. As regards reaction times, in contrast, there was a significant difference among the two-argument conditions in the Other group [$F(2,12) = 4.2$, $P = 0.042$] and normal control subjects [$F(2,54) = 4.6$, $P = 0.014$], but neither in the LPMC group [$F(2,12) = 0.43$, $P = 0.66$] nor in the F3 group [$F(2,12) = 0.16$, $P = 0.85$]. In both the Other group and normal control subjects, the reaction times were significantly longer under the scrambled than the active sentence condition (corrected $P < 0.05$), normally distinguishing these two conditions.

Activation of the syntax-related regions in normal participants

For the functional MRI data, each subtracted side of a contrast between two conditions (e.g. two-argument out of the

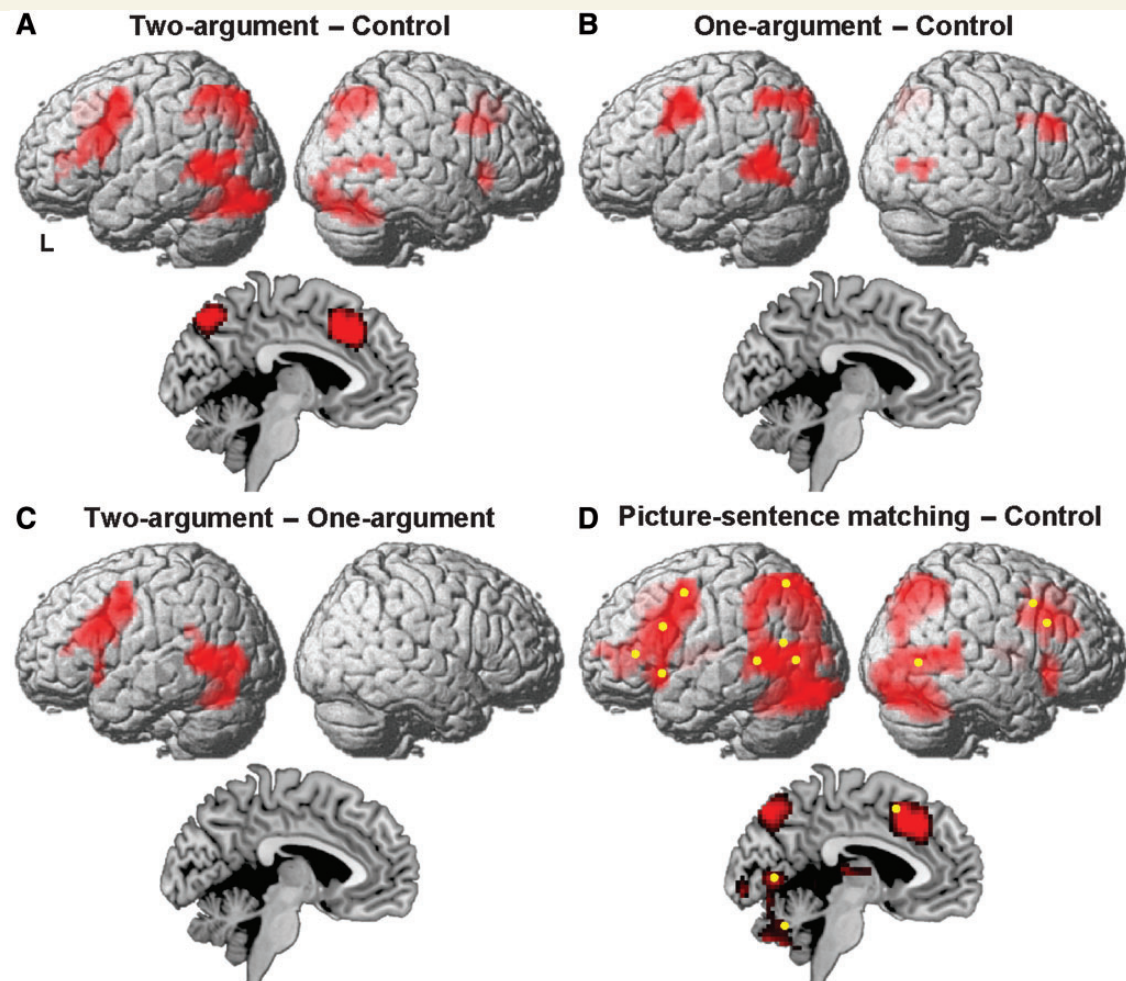


Figure 2 Reanalyses of previous data for normal participants ($n = 14$) (Kinno *et al.*, 2008). Significant regions were identified by the Two-argument – Control (A), One-argument – Control (B), Two-argument – One-argument (C), and Picture-sentence matching – Control (D) contrasts. The results of paired t -test were thresholded at $P < 0.005$ for the voxel level, and at corrected $P < 0.05$ for the cluster level, with family-wise error correction across the whole brain using SPM2. See Supplementary Table 1 for the stereotactic coordinates of the activation foci (A–C). Each yellow dot represents the local maximum of an activated region shown in Fig. 7, all of which were included in the regions identified by the Picture-sentence matching – Control contrast shown here. L = left.

'Two-argument – One-argument' contrast) was compared between trials with correct and incorrect responses beforehand in a first-level analysis of each participant [e.g. Two-argument (correct – incorrect) – One-argument (all trials)]. This procedure removed any effects of abnormal medical conditions (e.g. anxiety-tension state), that were included in both correct and incorrect responses, as much as possible from cortical activations. For a separate examination of trials with correct and incorrect responses [e.g. Two-argument (correct or incorrect) – One-argument (all trials)], the use of an identical reference was mandatory for an exact comparison of both trial types (Fig. 7B), preferably including both correct and incorrect trials in the subtracting side. Therefore, we used the same reference of one-argument (all trials) for a comparison with Two-argument (correct – incorrect) as well (see Fig. 7A). We also confirmed that the Two-argument (correct – incorrect) – One-argument (correct – incorrect) contrast resulted in the same activation patterns presented here.

Here we reanalysed the previous functional MRI data taken from 14 normal participants (Kinno *et al.*, 2008), in which we had used different MRI acquisition parameters and a shorter intratrial interval (3800 ms instead of 5800 ms). We first tested the Two-argument – Control contrast (Fig. 2A and Supplementary Table 1). This contrast revealed significant activation in the bilateral regions of the LPMC, opercular/triangular/orbital parts of the F3, posterior superior/middle/inferior temporal gyri, angular gyrus, and intraparietal sulcus, as well as in the presupplementary motor area and precuneus. In the One-argument – Control contrast, significant activation was limited to the bilateral regions of the LPMC and posterior superior/middle temporal gyri, as well as the left intraparietal sulcus (Fig. 2B), whereas in the Two-argument – One-argument contrast, activation was clearly localized in the left frontal and temporal regions alone (Fig. 2C). To visualize an overall activation pattern in the normal participants, we also tested the Picture-sentence matching – Control contrast (Fig. 2D; see

Fig. 1A for the tasks), which exhibited activation in all of the regions mentioned above, together with lingual gyrus and cerebellar nuclei.

To set the same sensitivity of signal-to-noise ratio for functional MRI maps of all tested groups, we equated the number of participants in each group. According to a Dunnett test, there was no significant difference in age and laterality quotient of handedness between the normal group (laterality quotient, 93 ± 13.0) and each patient group (corrected $P > 0.4$). All of the following functional MRI results were based on the present data taken from the normal group and patient groups.

Loss of activation modulation in the syntax-related regions of agrammatic patients

We assessed differences in activation among the patient groups by performing an analysis of covariance with two factors [Group (LPMC, F3, Other) \times Condition (active, passive, scrambled)]. A significant main effect of group was observed in the opercular/triangular/orbital parts of the left F3 (corrected $P < 0.05$) (Fig. 3A and Supplementary Table 2), probably reflecting the underactivity and/or overactivity of these regions as a result of lesions in some patient groups. We also found a significant interaction of group by condition in the left LPMC, in the opercular/triangular/orbital parts of the left F3, and in the left posterior superior/middle temporal gyri (Fig. 3B). These regions were all left-lateralized and actually recruited in normal sentence processing (Fig. 2C). On the other hand, there was no significant main effect of condition in any regions; any such effect was likely masked by the condition-independent responses in some patient groups.

To further clarify the activation modulation among the two-argument conditions, the per cent signal changes were calculated at the local maxima of the left frontal and temporal regions in Fig. 3B. In the normal group, a repeated measures ANOVA with two factors [Condition (active, passive, scrambled) \times Region (LPMC, opercular/triangular, orbital, temporal)] revealed a strong main effect of condition [$F(2,12) = 20$, $P = 0.0002$] and a marginal main effect of region [$F(3,18) = 3.2$, $P = 0.050$], with no interaction [$F(6,36) = 1.4$, $P = 0.23$]. According to a Bonferroni/Dunn test, the signal changes in the left LPMC were significantly higher under the scrambled than under the active sentence condition (corrected $P < 0.05$) (Fig. 3C). The signal changes in the opercular/triangular parts of the left F3, as well as those in the orbital part of the left F3, were significantly higher under the passive and scrambled than under the active sentence conditions (Fig. 3D and E), whereas those in the left posterior superior/middle temporal gyri were significantly higher under the scrambled than under the active and passive sentence conditions (Fig. 3F). These modulation patterns of activations precisely replicated our previous results in the normal participants (Kinno *et al.*, 2008), indicating that these crucial regions work in concert to process sentences, with their respective contributions being dynamically regulated by syntactic requirements.

In the Other group, a strong main effect of condition [$F(2,12) = 33$, $P < 0.0001$], as well as a marginal main effect of

region [$F(3,18) = 3.2$, $P = 0.050$], was observed with no interaction [$F(6,36) = 1.9$, $P = 0.12$]. According to a Bonferroni/Dunn test, the activation modulation among the two-argument conditions in the Other group exactly replicated that in the normal group (corrected $P < 0.05$). In both the LPMC and F3 groups, in contrast, the activation modulation in these four regions was completely lost (Fig. 3C–F), with no significant main effect of condition ($P > 0.3$). It is striking to note that, in the F3 group, activation was absent in all of these regions. These results suggest that the loss of activation modulation in these regions is a good indicator of agrammatic comprehension.

Syntax-related activation patterns in the normal group

For the normal group, we first examined the Two-argument – Control contrast (Fig. 4A and Supplementary Table 2), which reproduced significant activation in the bilateral regions of the LPMC and posterior superior/middle temporal gyri, as well as in the orbital part of the left F3, presupplementary motor area, left posterior middle/inferior temporal gyri, and left intraparietal sulcus. The absence of significant activation in the right intraparietal sulcus and precuneus, etc., which was present in Fig. 2A, may be because of a reduced sensitivity of signal-to-noise ratio for the smaller population and/or a longer (i.e. less demanding) intratrial interval.

Even in the more stringent contrast of Two-argument – One-argument, all participants in the normal group showed consistently left-lateralized activation in the left frontal and temporal regions (Fig. 4B). Notable idiosyncrasy was restricted to weaker activation in the right frontal and presupplementary motor area for a few participants. Moreover, the group analysis in this contrast showed clearly left-lateralized activations in the left frontal and temporal regions (Fig. 5A and Supplementary Table 3), consistent with the result shown in Fig. 2C. It is notable that significant activation was absent in the right or medial regions in the normal brain.

Abnormal overactivity in the LPMC group for correct responses alone

In the Two-argument – One-argument contrast, the LPMC group showed activation in the left frontal (ventrally expanded) and temporal regions, as well as additional activation in the left intraparietal sulcus, right frontal regions, presupplementary motor area, and right temporal regions (Fig. 5B). It is striking to note that this activation pattern was similar to that in the normal brain for the Two-argument – Control contrast (Fig. 4A). Moreover, these regions were consistently observed for all patients in the LPMC group (Fig. 6A). The only notable idiosyncrasies were the enhanced activation in the right ventral frontal regions for Patient 1, and the absence of activation in the left intraparietal sulcus for Patient 3. As the observed abnormal overactivity in the LPMC group was selective to correct responses, these compensatory changes were coupled with task demands under the two-argument conditions.

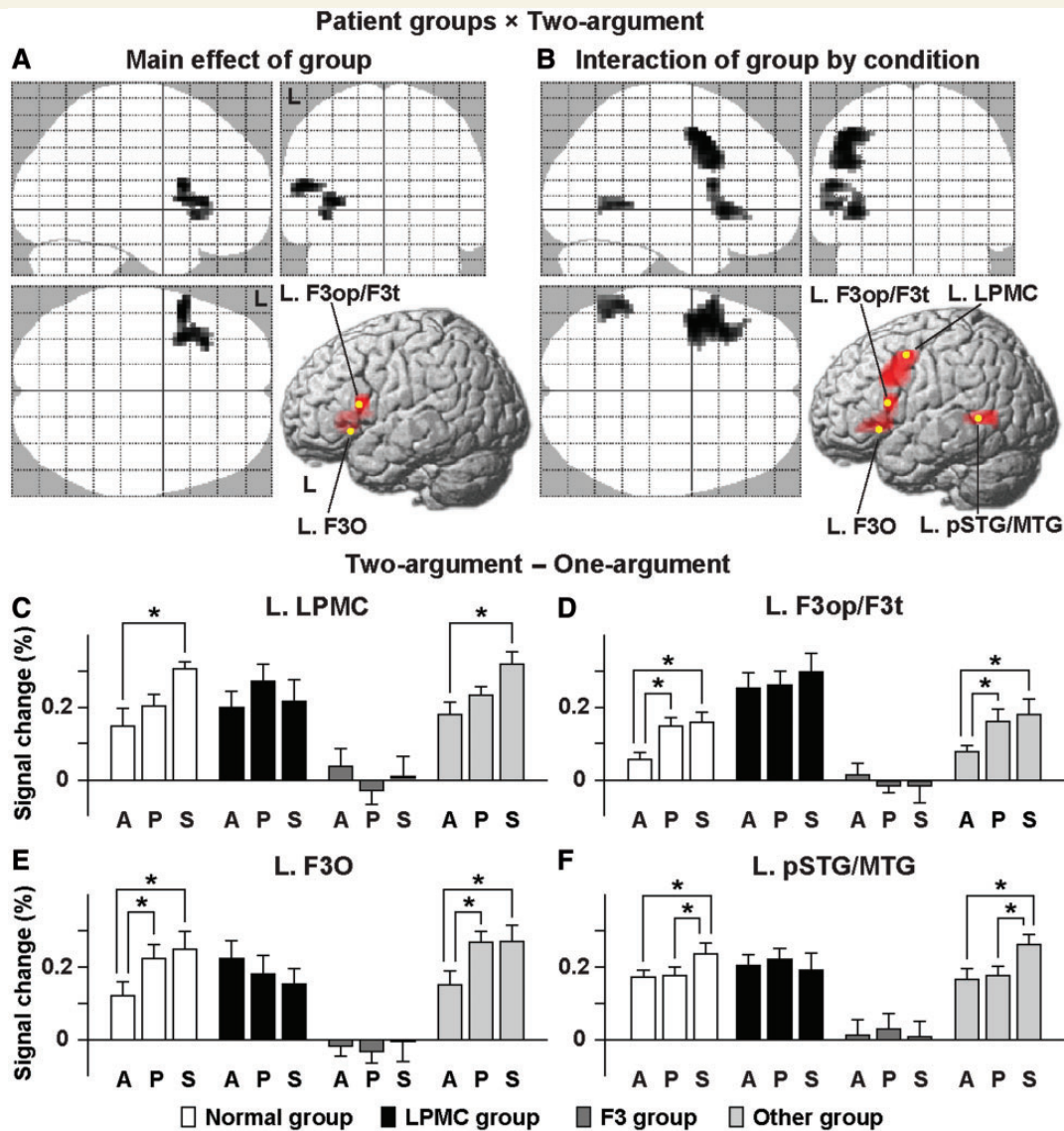


Figure 3 Differential activation modulation among the two-argument conditions. (A and B) Significant regions identified by an analysis of covariance with two factors [Group (LPMC, F3, Other) × Condition (active, passive, scrambled)], which were projected in three orthogonal planes (sagittal, coronal, and axial from the *top left* panel) and onto the left surface-rendered standard brain. There was a significant main effect of group in the left frontal regions (A), as well as a significant interaction of group by condition in the four left regions (B). See Supplementary Table 2 for the stereotactic coordinates of the activation foci. Each yellow dot indicates the local maximum of an activated region. (C–F) Histograms for the per cent signal changes at the local maxima of the left LPMC (C), opercular/triangular parts of the left F3 (D), orbital part of the left F3 (E), and left posterior superior/middle temporal gyri (F). The per cent signal changes for the active, passive, and scrambled sentence conditions are shown with reference to the one-argument condition (all trials). Error bars indicate the standard error of the mean for the participants, and asterisks denote the significant differences among the two-argument conditions (corrected $P < 0.05$). Note that the activation modulation in the four regions, which was observed in the normal and Other groups, was completely lost for the LPMC and F3 groups, i.e. agrammatic patients. A = active sentence condition; F3O = orbital part of the F3; F3op/F3t = opercular/triangular parts of the F3; L = left; P = passive sentence condition; pSTG/MTG = posterior superior/middle temporal gyri; S = scrambled sentence condition.

Abnormal overactivity in the F3 group for both correct and incorrect responses

In the F3 group, it is striking to note that the Two-argument – One-argument contrast induced no significant activation in the whole brain (Fig. 5C). These radically differential

activation patterns between the LPMC and F3 groups indicate distinct abnormal changes in activation. In contrast, the activation pattern in the Other group (Fig. 5D) was similar to that in the normal group. Indeed, all patients in the Other group showed consistent activation in mostly the left frontal and temporal regions (Fig. 6B). Notable idiosyncrasy was restricted to the

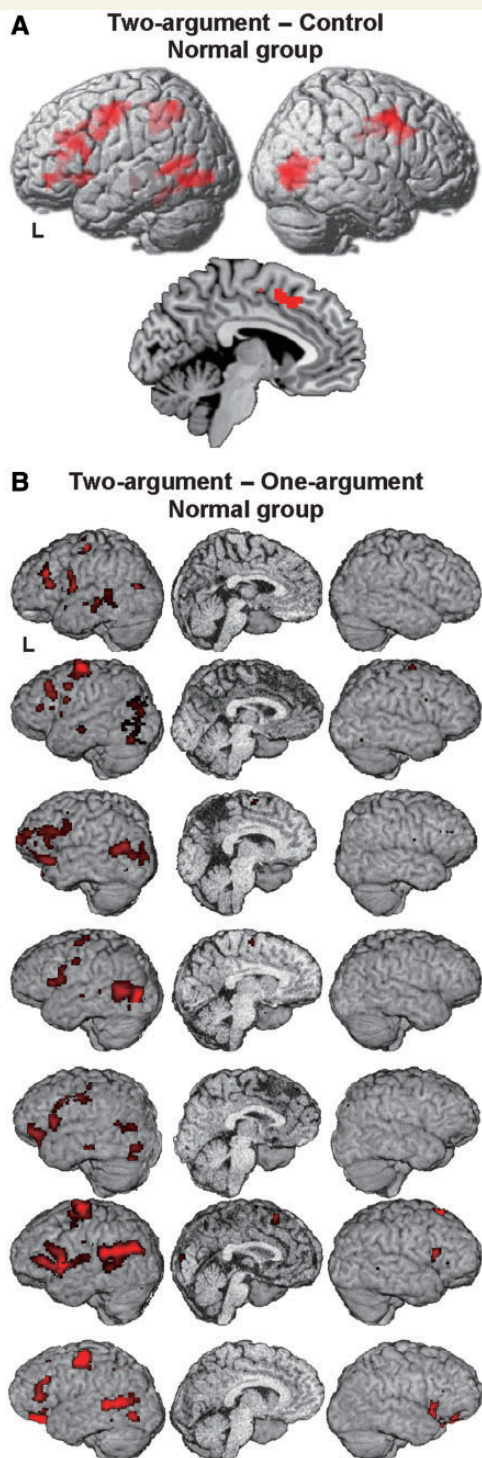


Figure 4 Syntax-related activation patterns in the normal group. (A) Significant regions identified by the Two-argument – Control contrast (paired *t*-test) for the normal group, which were projected onto the left and right lateral surfaces of the standard brain. Medial sections are also shown. See Supplementary Table 2 for the stereotactic coordinates of the activation foci. (B) Significant regions identified by the Two-argument – One-argument contrast for each participant in the normal group. Activations were projected onto the left and right lateral surfaces of each individual brain. Individual medial sections are also shown. The threshold was set at $P < 0.005$ for the voxel level. All normal participants showed consistent activation in the left frontal and temporal regions. L = left.

activation in the right hemisphere for some patients, which was much less prominent than that in the LPMC group.

The absence of significant activation in the F3 group may have been because of comparable activations between the two-argument and one-argument conditions, or those between correct and incorrect responses. The Two-argument – One-argument contrast was thus further examined separately for trials with correct and incorrect responses under the two-argument conditions. In the normal group, the activation pattern for correct responses alone (Fig. 5E and Supplementary Table 4) exactly replicated that shown in Fig. 5A; there was no significant activation for incorrect responses in the whole brain (Fig. 5F). In contrast, we observed unique activation patterns in the F3 group, such that the left LPMC, left angular gyrus, lingual gyrus, and cerebellar nuclei showed consistent overactivity for both correct (Fig. 5G) and incorrect (Fig. 5H) responses. These activation patterns for both correct and incorrect responses were consistently observed for all patients in the F3 group (Fig. 6C and D). Notable idiosyncrasy was restricted to activation in the right parietal and occipital regions for Patient 9, and to activation in the presupplementary motor area for Patient 10; the activation patterns for correct and incorrect responses were exactly the same even for these two patients.

Here we should note that both behavioural and activation data were basically consistent among the patients within each of the patient groups (Table 2 and Fig. 6), excluding any modulation as a result of tumour grade and/or gender. Therefore, tumour location was the only factor that differentiated the three patient groups. Moreover, our results indicate that the activation patterns were both quantitatively and qualitatively different between the LPMC and F3 groups, particularly with respect to the activations for correct and incorrect responses.

Multiple regions with abnormal overactivity or underactivity

To precisely quantify overactivity and/or underactivity in the LPMC and F3 groups, the per cent signal changes in the Two-argument – One-argument contrast were calculated at the local maxima of the 14 regions shown in Fig. 5 (yellow dots), all of which were included in the regions revealed by the Picture–sentence matching – Control contrast for the normal participants (Fig. 2D). As some activated regions were more focal and enhanced in the patient groups, we took some regions from the patients' activation maps, all of which were clearly outside the lesions: the left frontal and temporal regions from the normal group (Fig. 5A and Supplementary Table 3), the left intraparietal sulcus, right frontal regions, presupplementary motor area, right temporal regions from the LPMC group (Fig. 5B and Supplementary Table 3), and the left angular gyrus, lingual gyrus, cerebellar nuclei from the F3 group (Fig. 5G and Supplementary Table 4).

For each region with increased activation in the LPMC group, a Dunnett test between the LPMC and normal groups showed significant overactivity (corrected $P < 0.05$; red asterisks in Fig. 7A). For each region with decreased activation in the F3 group, a Dunnett test between the F3 and normal groups showed

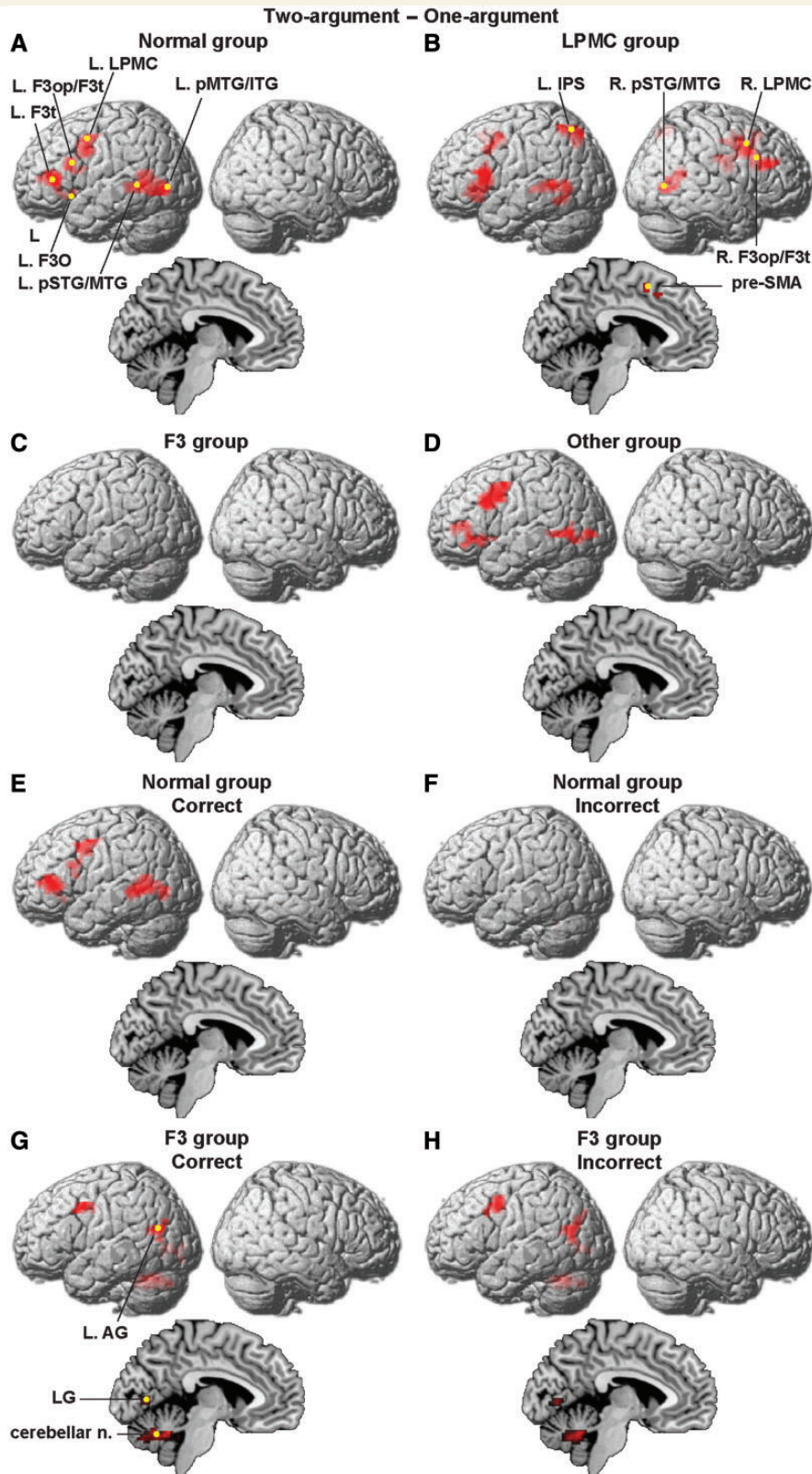


Figure 5 Differential activation patterns in the patient groups. (A–D) Significant regions identified by the Two-argument – One-argument contrast for the normal group (A), LPMC group (B), F3 group (C), and Other group (D). See Supplementary Table 3 for the stereotactic coordinates of the activation foci. The normal and Other groups showed clearly left-lateralized activation. In contrast, the LPMC group showed overactivity in both hemispheres, whereas the F3 group showed no significant activation at all. (E and F) Significant regions identified by the Two-argument – One-argument contrast for the normal group, shown separately for correct (E) and incorrect (F) responses. See Supplementary Table 4 for the stereotactic coordinates of the activation foci. (G and H) Significant regions identified by the

(continued)

significant underactivity (green asterisks in Fig. 7A) except the left posterior middle/inferior temporal gyri. In the F3 group, it is striking to note that the signal changes for correct and incorrect responses were exactly the same in all 14 of the regions examined (Fig. 7B). For each region with increased activation in the F3 group (i.e. left LPMC, left angular gyrus, lingual gyrus, and cerebellar nuclei), a Dunnett test between the F3 and normal groups showed significant overactivity for both correct and incorrect responses (black asterisks in Fig. 7B). In contrast, the other left frontal and temporal regions, including the left posterior middle/inferior temporal gyri, showed significant underactivity for correct responses (green asterisks in Fig. 7B).

Three networks of regions based on the functional connectivity

Based on the functional connectivity among the 14 syntax-related regions, we identified normal networks with direct connections by using a partial correlation method (Smith, 2012). Figure 7C shows a partial correlation matrix and network-boundary effects, which clearly revealed three separated networks in the normal brain. We confirmed that there was no negative correlation within individual networks. The non-diagonal correlations within individual networks were significantly greater than those between any of two networks ($P < 0.0001$; see the bar graph in Fig. 7C). We named the largest network as Network I, the second-largest and more widespread network as Network II, and the remaining network as Network III (Fig. 7D).

Network I consists of the opercular/triangular parts of the left F3, left intraparietal sulcus, right LPMC, opercular/triangular parts of the right F3, presupplementary motor area, and right posterior superior/middle temporal gyri, all of which were overactivated in the LPMC group selective for correct responses. Network II consists of the left LPMC, left angular gyrus, lingual gyrus, and cerebellar nuclei, all of which were overactivated in the F3 group for both correct and incorrect responses. Network III consists of the triangular part of the left F3, orbital part of the left F3, left posterior superior/middle temporal gyri, and left posterior middle/inferior temporal gyri, all of which were underactivated in the F3 group for correct responses. These results clearly demonstrate that the three networks are functionally distinct in the normal circuitry subserving syntactic processing (Table 3). Moreover, it is striking to note that these normal networks were differentially recruited by the LPMC and F3 groups leading to abnormal overactivity and underactivity.

Anatomical connections for the syntax-related networks

We used diffusion tensor imaging with probabilistic tractography in the normal brain to further examine which of the dorsal and ventral tracts are actually integrated into each of these syntax-related networks. Seed masks were placed at the 14 regions in the following nine pairs: the opercular/triangular parts of the left F3 and those of the right F3; the opercular/triangular parts of the left F3 and left intraparietal sulcus; the left intraparietal sulcus and right posterior superior/middle temporal gyri; the opercular/triangular parts of the right F3 and right posterior superior/middle temporal gyri; the opercular/triangular parts of the right F3 and presupplementary motor area; the left LPMC and left angular gyrus; the left LPMC and cerebellar nuclei; the left angular gyrus and lingual gyrus; and the triangular part of the left F3 and left posterior middle/inferior temporal gyri. The tracts connecting other pairs of regions were basically covered by the examined pairs.

We identified a single largest cluster that connected two regions, together with much smaller clusters or islands (Fig. 8A–C). For Network I, the anterior corpus callosum connected the opercular/triangular parts of the left F3 and those of the right F3, whereas the splenium of corpus callosum connected the left intraparietal sulcus and right posterior superior/middle temporal gyri. Our tractography did not consistently connect the opercular/triangular parts of the left F3 and the left intraparietal sulcus. On the other hand, the right dorsal pathway of the arcuate and superior longitudinal fasciculi connected the right frontal and temporal regions. The opercular/triangular parts of the right F3 were also directly connected to the presupplementary motor area. For Network II, the left dorsal pathway of the arcuate and superior longitudinal fasciculi connected the left LPMC and left angular gyrus, and reached the left posterior superior/middle temporal gyri. Moreover, the left LPMC and cerebellar nuclei were connected via the thalamus, whereas the left angular gyrus and lingual gyrus were directly connected. For Network III, the left ventral pathway of the middle longitudinal fasciculus and extreme capsule connected the left ventral frontal and posterior temporal regions, and reached the left angular gyrus. It is notable that most of these anatomical connections, especially those within Network II, were consistent with the higher values of partial correlations in the functional connectivity (Fig. 7C). These results are summarized in Fig. 8D, and further demonstrate that the wide-ranging fibres of the three networks were also anatomically distinct and penetrated both the cerebral hemispheres and left cerebellum.

Figure 5 Continued

Two-argument – One-argument contrast for the F3 group, shown separately for correct (G) and incorrect (H) responses. Note the consistent overactivity in the left LPMC, left angular gyrus, lingual gyrus, and cerebellar nuclei for both correct and incorrect responses. Each yellow dot represents the local maximum of an activated region used for the later analyses. AG = angular gyrus; F3O = orbital part of the F3; F3op/F3t = opercular/triangular parts of the F3; F3t = triangular part of the F3; IPS = intraparietal sulcus; L = left; LG = lingual gyrus; n. = nuclei; pMTG/ITG = posterior middle/inferior temporal gyri; pre-SMA = presupplementary motor area; pSTG/MTG = posterior superior/middle temporal gyri; R = right.

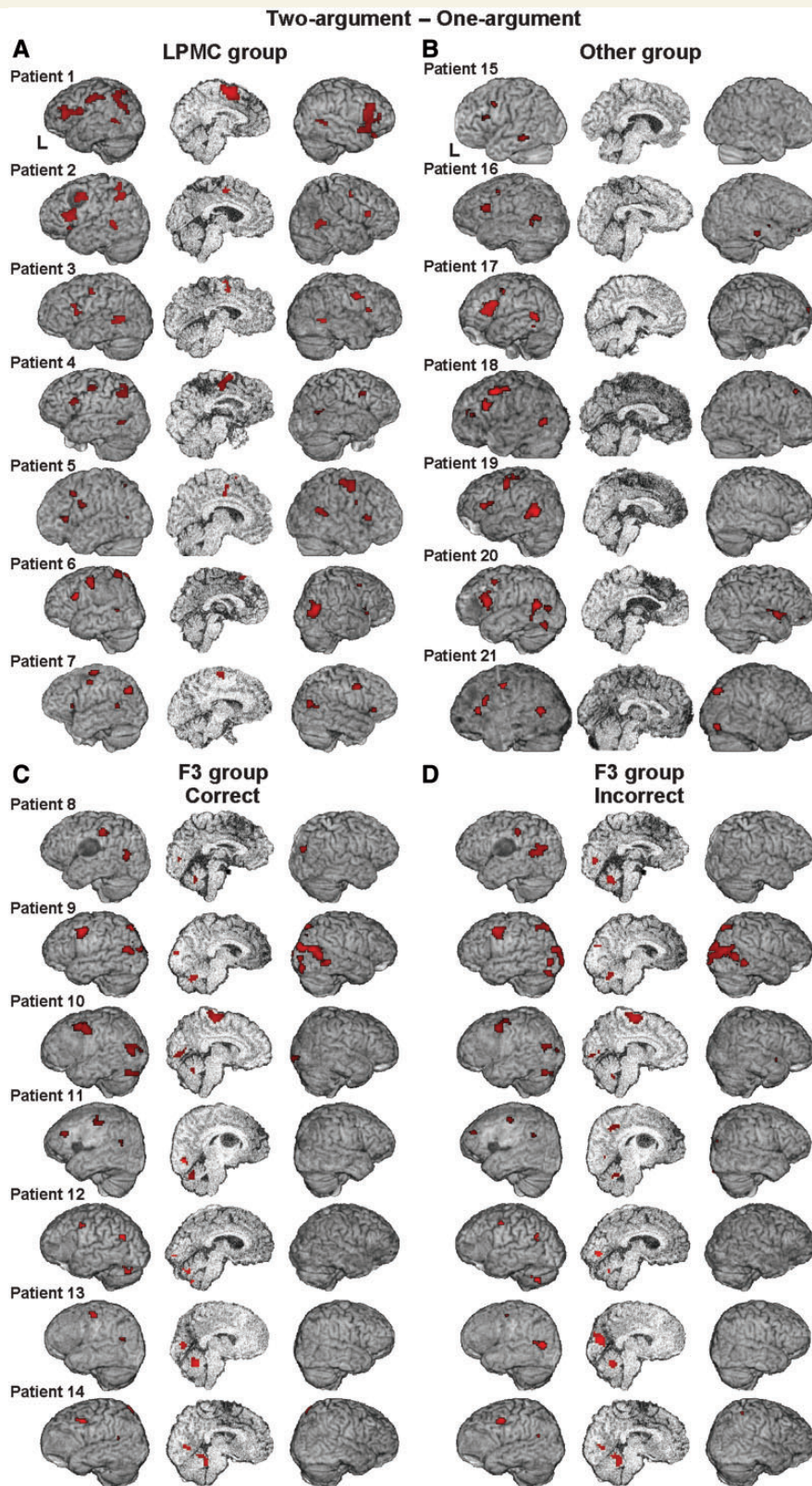


Figure 6 Consistently activated regions within each patient group. (A and B) Significant regions identified by the Two-argument – One-argument contrast for each patient in the LPMC group (Patients 1–7, see Table 1) (A), and in the Other group (Patients 15–21) (B). Activations were projected onto the left and right lateral surfaces of each individual brain. Individual medial sections are also shown. The threshold was set at $P < 0.005$ for the voxel level. All patients in the LPMC group showed consistent activation in the bilateral frontal and temporal regions, as well as in the presupplementary motor area and left intraparietal sulcus. In contrast, all patients in the Other group showed consistent activation in mostly the left frontal and temporal regions, as in the normal group (Fig. 5A). (C and D) Significant regions identified by the Two-argument – One-argument contrast for each patient in the F3 group (Patients 8–14), shown separately for correct (C) and incorrect (D) responses. All patients in the F3 group showed consistent overactivity in the left LPMC, left angular gyrus, lingual gyrus, and cerebellar nuclei for both correct and incorrect responses. L = left.

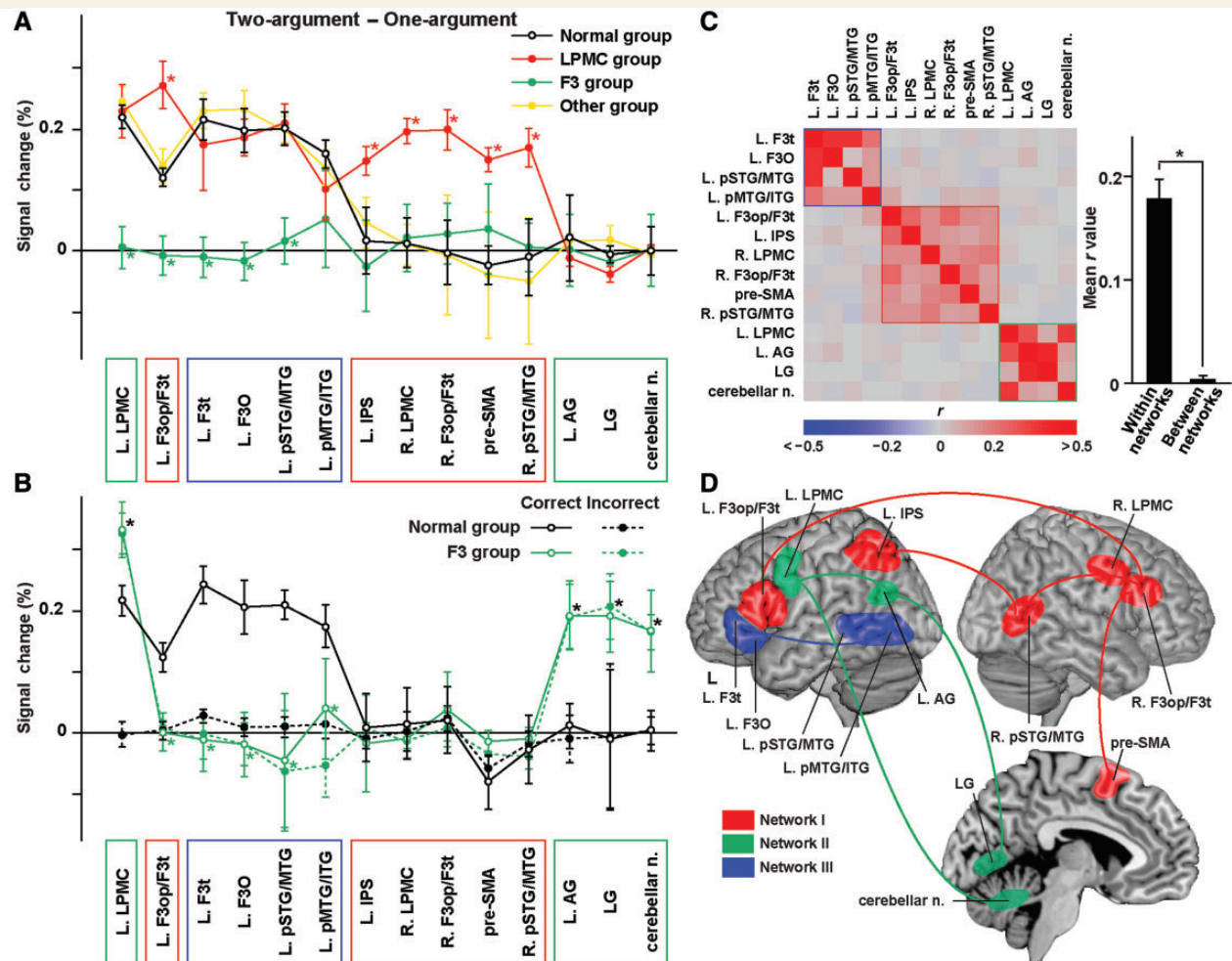


Figure 7 Abnormal overactivity and/or underactivity of the three syntax-related networks. (A) Per cent signal changes in the Two-argument – One-argument contrast at the local maxima of 14 regions. Error bars indicate the standard error of the mean for the participants. Asterisks denote significant differences from the normal group (corrected $P < 0.05$), which consisted of either overactivity in the LPMC group or underactivity in the F3 group. (B) Per cent signal changes in the Two-argument – One-argument contrast, shown separately for correct and incorrect responses in the F3 and normal groups. For the correct responses, asterisks denote significant differences between the two groups (corrected $P < 0.05$), indicating overactivity for correct and incorrect responses, as well as underactivity for correct responses. (C) A partial correlation matrix and network-boundary effects for the normal participants. The 14 regions were arranged in the order of Fig. 7A and B, except the left LPMC and opercular/triangular parts of the left F3. As in Fig. 7A and B, the three networks surrounded by red, green, and blue boxes correspond to the Networks I, II, and III, respectively. (D) Schematic of the three syntax-related networks in the normal brain. The brain regions for Networks I, II, and III are shown in red, green, and blue, respectively. Note that these three networks involve the opercular/triangular parts of the left F3, left LPMC, and orbital part of the left F3 in the left frontal cortex, respectively (Table 3). Connections within individual networks are shown with coloured lines. AG = angular gyrus; F3O = orbital part of the F3; F3op/F3t = opercular/triangular parts of the F3; F3t = triangular part of the F3; IPS = intraparietal sulcus; L = left; LG = lingual gyrus; n. = nuclei; pMTG/ITG = posterior middle/inferior temporal gyri; pre-SMA = presupplementary motor area; pSTG/MTG = posterior superior/middle temporal gyri; R = right.

Discussion

We established two qualitatively different types of agrammatic comprehension, depending on glioma location (Fig. 1C and D). By comparing the activation patterns among the three patient groups and the normal group, we observed that the activation modulation under the two-argument conditions was completely lost in the syntax-related regions in the LPMC and F3 groups (Fig. 3C–F). Moreover, we found dramatic changes in the

activation patterns for both groups (Fig. 5), which accompanied abnormal overactivity and/or underactivity in the syntax-related regions (Fig. 7A and B). Furthermore, by examining functional connectivity in the normal brain, we identified three syntax-related networks among those regions (Fig. 7C), and anatomically visualized connections within individual networks (Fig. 8). These results demonstrate that agrammatic comprehension is associated with the global reorganization of functionally distinct networks, which indeed reflects a differential change in the relative

Table 3 Summary of the normal and abnormal activity in each syntax-related network

Network	Left frontal regions included	Two-argument – Control	Two-argument – One-argument			Possible normal functions
		Normal group	Normal group	LPMC group	F3 group	
I	L. F3op/F3t	+	±	++	–	Syntax and its supportive system
II	L. LPMC	±	±	±	++	Syntax and input/output interface
III	L. F3t, L. F3O	+	+	+	–	Syntax and semantics

Significant activations are schematically presented: +, normal activity as a whole network; ++, abnormal overactivity as a whole network; –, abnormal underactivity as a whole network; ±, significant activity in the left frontal regions alone, which was dependent on the reference conditions (control or one-argument; see Network I). See Fig. 4A for the Two-argument – Control contrast; see Fig. 5A, B, D, and G for the Two-argument – One-argument contrast.

F3O = orbital part of the F3; F3op/F3t = opercular/triangular parts of the F3; F3t = triangular part of the F3; L = left.

contribution of these three networks to normal syntax-related functions (Table 3).

Based on the overview of cognitive and neuronal (i.e. anatomical) changes by Price and Friston (1999), it is probable that abnormal overactivity of Network I in the LPMC group reflected a cognitive change. This overactivity suggests a compensatory change in cognitive architecture because of the increased demands on normal processes, because the overactivity mimicked the activation pattern in the Two-argument – Control contrast (i.e. contrasted with the lower control) in the normal group (Fig. 4A). As regards Network II, signal changes for correct responses were exactly the same as those for incorrect responses in the F3 group (Fig. 7B), independent of cognitive factors, suggesting that its overactivity reflected a neuronal change due to the disconnection or disinhibition of a duplicate (degenerate) system. The underactivity of Network III in the F3 group indicates another neuronal change leading to diaschisis in the left temporal cortex.

The functions of these three networks can be inferred by integrating the possible roles of individual regions suggested by previous studies into the present results. First of all, the complementary overactivity observed between the left LPMC and the opercular/triangular parts of the left F3 (Table 3) is consistent with the critical roles of both regions in syntactic processing (Hashimoto and Sakai, 2002; Bornkessel *et al.*, 2005; Kinno *et al.*, 2008, 2009). Network I included not only the opercular/triangular parts of the left F3, but right frontal and temporal regions. A previous study has reported functional roles of right frontal and temporal regions for repairing syntactically incorrect sentences (Meyer *et al.*, 2000), suggesting that these right regions would be related to a supportive system for syntactic processing. As shown in Fig. 8A, the right dorsal pathway of the arcuate and superior longitudinal fasciculi connected the right frontal and temporal regions. It has been suggested that this right pathway is important for an artificial rule learning of pitch patterns (Loui *et al.*, 2011), which may also have a supportive role for processing linguistic stimuli. As regards the posterior corpus callosum between the left intraparietal sulcus and right superior/middle temporal gyri, previous studies have reported its functional roles for utilizing prosodic cues supportively for processing auditory presented sentences (Friederici *et al.*, 2007). The presupplementary motor area, as well as the pathway between the presupplementary motor area and right LPMC may have another supportive role, as suggested by transient speech disorders due to a resection of the medial

frontal lesions including these regions (Krainik *et al.*, 2003). Taken together, Network I would be related to syntax and its supportive system.

Network II included the left dorsal pathway connecting the left LPMC and left angular gyrus, and this pathway reached the left posterior superior/middle temporal gyri. A previous study has suggested that the dorsal pathway connecting the LPMC and temporal gyrus is important for 'sensory to motor mapping' rather than for 'semantic and syntactic functions' (Friederici, 2011). Although the functional role of the dorsal pathway remains controversial, this and other pathways included in Network II may function as the interface between sensory input and motor output. As shown in Fig. 8B, the connection between the left angular gyrus and lingual gyrus was also included in Network II. Previous studies have reported significant activation in the left angular gyrus for searching the semantic features of visually presented words and pictures (Seghier *et al.*, 2010), and that in the lingual gyrus for memorizing visually presented phrases (Hashimoto and Sakai, 2002). A previous PET study with dyslexic patients has shown the importance of the functional connectivity between these two regions for single-word reading abilities (Horwitz *et al.*, 1998), suggesting the significance of this pathway for the visual input. Network II further included the connection between the left LPMC and cerebellar nuclei via the thalamus. The deep cerebellar nuclei has been considered a part of a widespread network including the frontal regions and thalamus for motor outputs (Habas, 2010), which has been anatomically confirmed (Behrens *et al.*, 2003; Granziera *et al.*, 2009). The resection of cerebellum tumours located in the midline often causes posterior fossa syndrome, including cognitive deficits and cerebellar mutism, i.e. speech output problems (Mariën *et al.*, 2013). It has been reported that a lesion in the dentate-thalamo-cortical tract leads to cerebello-cerebral diaschisis and subsequent mutism (Küper and Timmann, 2013). Taken together, Network II would be related to syntax and input/output interface for linguistic processing.

Network III consisted of the triangular/orbital parts of the left F3 and left posterior superior/middle/inferior temporal gyri. Previous studies have suggested that the orbital part of the left F3 is selectively involved in the semantic processing of sentences (Homae *et al.*, 2002), and that the left posterior superior/middle temporal gyri are related to both syntactic and semantic processing (Friederici *et al.*, 2003; Suzuki and Sakai, 2003; Kinno *et al.*, 2008). These findings suggest that the left ventral frontal and

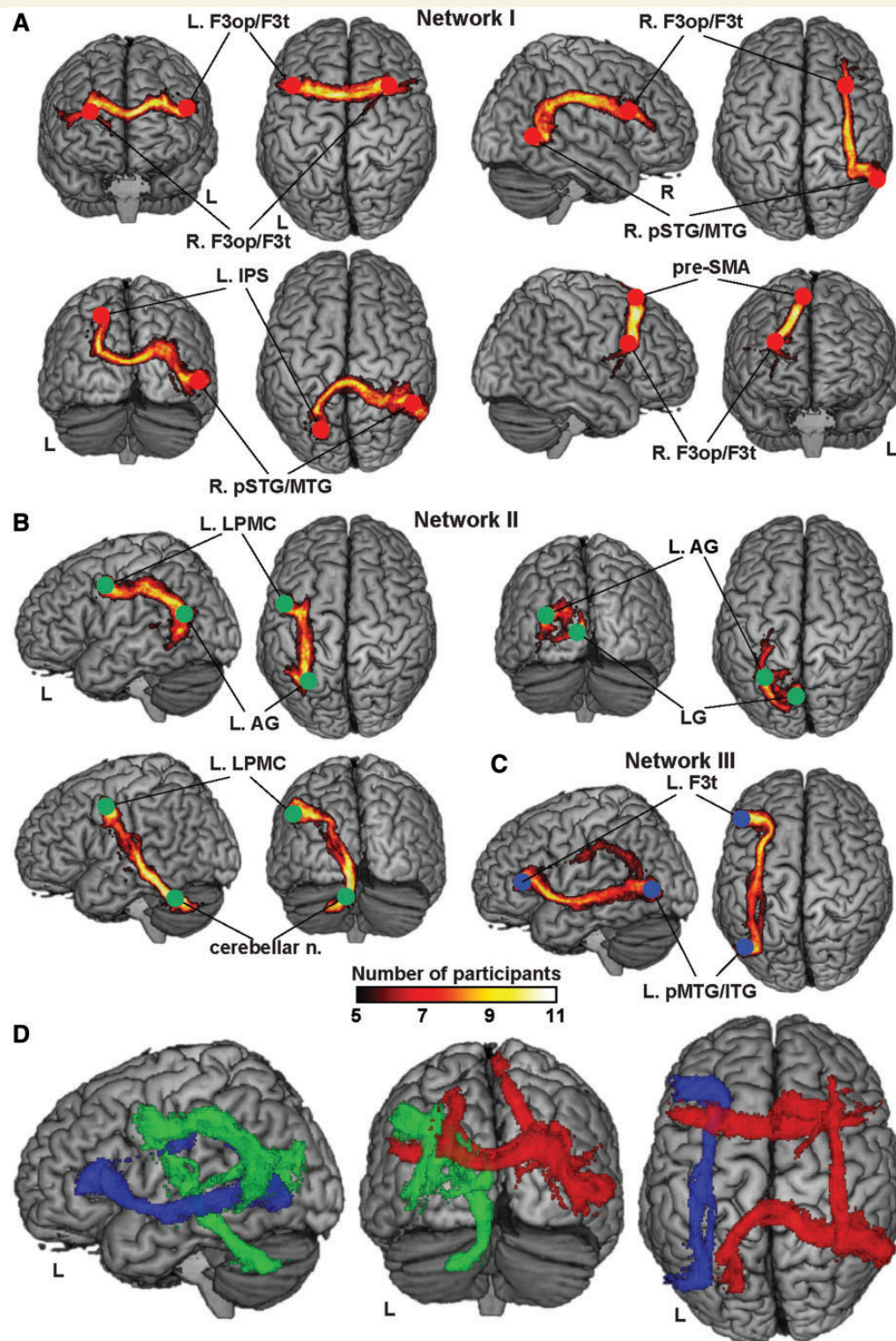


Figure 8 Anatomical connections for the syntax-related networks in the normal brain. Based on the results with diffusion tensor imaging, the population probability maps are shown on the left/right lateral, anterior/posterior, and dorsal surfaces of the standard brain with maximum intensity projection. Red, green, and blue spheres represent seed masks for Networks I, II, and III, respectively. The pathways have been thresholded to show only those present in at least 5 of 11 participants; the colour scale denotes the number of participants. (A–C) Fibres within Networks I (A), II (B), and III (C). (D) Perspective drawings of the three syntax-related networks. Fibres for two of Networks I (red), II (green), and III (blue) are shown in the left lateral, posterior, and dorsal views of the standard brain. More lateral, posterior, and dorsal fibres are shown in the upper layers of each panel. AG = angular gyrus; F3op/F3t = opercular/triangular parts of the F3; F3t = triangular part of the F3; IPS = intraparietal sulcus; L = left; LG = lingual gyrus; n. = nuclei; pMTG/ITG = posterior middle/inferior temporal gyri; pre-SMA = presupplementary motor area; pSTG/MTG = posterior superior/middle temporal gyri; R = right.

posterior temporal regions in Network III would be related to both syntax and semantic processing. As shown in Fig. 8C, the ventral route connected the triangular part of F3 and temporal gyrus. A previous lesion study has reported that the selective disconnection in this pathway caused deficits in sentence comprehension while lexical processing was left intact (Griffiths *et al.*, 2013). Taken together, Network III would be related to the syntax-semantic interaction. These three syntax-related networks with distinct functional roles in the normal brain thus separately connect key linguistic centres and work in concert to process sentences.

The patients in the LPMC group showed agrammatic comprehension (Fig. 1C), even though all of the regions of Network I were overactivated, whereas activations in Networks II and III remained normal (Fig. 7A). It is possible that such an increased contribution of the supportive system of network I could help partially overcome the deficit in the comprehension of passive sentences, which are marked in the verb morphology (-*areru*) and thus more salient than scrambled sentences. In contrast, the patients in the F3 group showed a different type of agrammatic comprehension (Fig. 1D), when all of the regions of Network III, as well as the opercular/triangular parts of the left F3 (i.e. the most crucial region that controls the other regions in Network I), were underactivated for correct responses (Fig. 7B). This deficit can be explained by noting that these patients failed to use the supportive function and syntax-semantic interaction, even though a neuronal change led to an increased contribution of the input/output interface of Network II. Therefore, the two types of agrammatic comprehension are consistent with the relative contribution of the three syntax-related networks.

In the neuropsychological literature, an opposing argument has been made that the study of brain tumours may not allow valid conclusions on the functional localization for the following reasons (Karnath and Steinbach, 2011). First, the diffuse spread of a tumour might extend beyond the tumour region as visualized by T₁-weighted or T₂-weighted MRI. In the present study, however, each lesion determined by MRI agreed well with the metabolic changes measured by ¹¹C-methionine, ¹⁸F-fluorodeoxyglucose, and ¹¹C-choline PET (Kato *et al.*, 2008). Second, normal function can be well preserved in the tumour region because of infiltration rather than destruction (Ojemann *et al.*, 1996; Krainik *et al.*, 2003). This point was not a problem in the present study, as we examined the whole brain, including the tumour region. We observed apparently normal left LPMC activations in the LPMC group (Fig. 7A), which could be a result of compensatory overactivation of remaining cells. Moreover, a brain shift caused by the mass effect of the tumour, if any, is limited to local activation changes, which cannot explain the global overactivity or underactivity. As a tumour may alter topographical landmarks of sulci, gyri, and ventricles, the location of a glioma could be estimated only approximately; we used a voxel-based approach of the Anatomical Automatic Labelling on normalized structural images for the approximate tumour location (Table 1). It is also difficult to delineate cortical areas even in normal participants because of the high variability of the gyrification in the inferior frontal gyrus. Our categorization criteria in the LPMC and F3 groups simply required voxel-based overlaps between a tumour and functional MRI data

on the normalized brains, without relying on topographical landmarks. In future studies, other methods such as surface-based semi-automated parcellation procedures would be helpful for the anatomical identification of regions on an individual's cortical map (Fischl *et al.*, 2004).

A previous functional MRI study on patients with the non-fluent variant of primary progressive aphasia (both the frontal and temporal regions were widely damaged) reported abnormal overactivity in the left posterior inferior frontal gyrus, as well as the absence of activation modulation due to 'syntactic complexity' (Wilson *et al.*, 2010), which seems consistent with our findings in the LPMC group. However, normal modulation was observed in the left mid-superior temporal sulcus in their patients in spite of the temporal lesions, which may reflect differences in other cognitive factors among the compared conditions. In our LPMC and F3 groups, the normal modulation in the left posterior superior/middle temporal gyri was clearly lost. It is likely that the loss of activation modulation in the left frontal regions was transmitted to other intact temporal regions in Network III.

According to the above discussion, the homotopic reorganization would have been the result of cognitive change, which was observed for all patients in the LPMC group, but not for any patients in the F3 or Other group (Fig. 6). A previous study has reported that aphasic patients showed overactivity in the right frontal regions for an auditory comprehension task, but only in the subacute phase after stroke (~2 weeks) (Saur *et al.*, 2006). Regarding the question of why homotopic reorganization occurs in a subset of patients (Desmurget *et al.*, 2007), our study suggests that homotopic reorganization actually depends on the location of a lesion. The differentiation and identification of the three syntax-related networks reported here would be a first step toward the elucidation of intricate networks uniquely specialized in the human brain for language processing.

Acknowledgements

We thank N. Komoro for technical assistance and H. Matsuda for administrative assistance.

Funding

This work was supported by a Core Research for Evolutional Science and Technology (CREST) grant from the Japan Science and Technology Agency (JST) and by a Grant-in-Aid for Scientific Research (S) (No. 20220005) / a Grant-in-Aid for Young Scientists (B) (No. 24720190) from the Ministry of Education, Culture, Sports, Science, and Technology of Japan.

Supplementary material

Supplementary material is available at *Brain* online.

References

- Behin A, Hoang-Xuan K, Carpentier AF, Delattre J-Y. Primary brain tumours in adults. *Lancet* 2003; 361: 323–31.
- Behrens TEJ, Johansen-Berg H, Woolrich MW, Smith SM, Wheeler-Kingshott CAM, Boulby PA, et al. Non-invasive mapping of connections between human thalamus and cortex using diffusion imaging. *Nat Neurosci* 2003; 6: 750–7.
- Bornkessel I, Zysset S, Friederici AD, von Cramon DY, Schleuwsky M. Who did what to whom? The neural basis of argument hierarchies during language comprehension. *Neuroimage* 2005; 26: 221–33.
- Caplan D, Baker C, Dehaut F. Syntactic determinants of sentence comprehension in aphasia. *Cognition* 1985; 21: 117–75.
- Dapretto M, Bookheimer SY. Form and content: dissociating syntax and semantics in sentence comprehension. *Neuron* 1999; 24: 427–32.
- Desmurget M, Bonnetblanc F, Duffau H. Contrasting acute and slow-growing lesions: a new door to brain plasticity. *Brain* 2007; 130: 898–914.
- Duffau H. Lessons from brain mapping in surgery for low-grade glioma: insights into associations between tumour and brain plasticity. *Lancet Neurol* 2005; 4: 476–86.
- Embick D, Marantz A, Miyashita Y, O'Neil W, Sakai KL. A syntactic specialization for Broca's area. *Proc Natl Acad Sci USA* 2000; 97: 6150–4.
- Fischl B, van der Kouwe A, Destrieux C, Halgren E, Ségonne F, Salat DH, et al. Automatically parcellating the human cerebral cortex. *Cereb Cortex* 2004; 14: 11–22.
- Friederici AD. The brain basis of language processing: from structure to function. *Physiol Rev* 2011; 91: 1357–92.
- Friederici AD, Rüschemeyer S-A, Hahne A, Fiebach CJ. The role of left inferior frontal and superior temporal cortex in sentence comprehension: localizing syntactic and semantic processes. *Cereb Cortex* 2003; 13: 170–7.
- Friederici AD, von Cramon DY, Kotz SA. Role of the corpus callosum in speech comprehension: interfacing syntax and prosody. *Neuron* 2007; 53: 135–45.
- Goodglass H, Menn L. Is agrammatism a unitary phenomenon? In: Kean M-L, editor. *Agrammatism*. Orlando, FL: Academic Press, 1985. p. 1–26.
- Granziera C, Schmahmann JD, Hadjikhani N, Meyer H, Meuli R, Wedeen V, et al. Diffusion spectrum imaging shows the structural basis of functional cerebellar circuits in the human cerebellum *in vivo*. *PLoS One* 2009; 4: e5101.
- Griffiths JD, Marslen-Wilson WD, Stamatakis EA, Tyler LK. Functional organization of the neural language system: dorsal and ventral pathways are critical for syntax. *Cereb Cortex* 2013; 23: 139–47.
- Grodzinsky Y. The neurology of syntax: language use without Broca's area. *Behav Brain Sci* 2000; 23: 1–71.
- Habas C. Functional imaging of the deep cerebellar nuclei: a review. *Cerebellum* 2010; 9: 22–8.
- Hashimoto R, Sakai KL. Specialization in the left prefrontal cortex for sentence comprehension. *Neuron* 2002; 35: 589–97.
- Homae F, Hashimoto R, Nakajima K, Miyashita Y, Sakai KL. From perception to sentence comprehension: the convergence of auditory and visual information of language in the left inferior frontal cortex. *Neuroimage* 2002; 16: 883–900.
- Horwitz B, Rumsey JM, Donohue BC. Functional connectivity of the angular gyrus in normal reading and dyslexia. *Proc Natl Acad Sci USA* 1998; 95: 8939–44.
- Karnath H-O, Steinbach JP. Do brain tumours allow valid conclusions on the localisation of human brain functions? - Objections. *Cortex* 2011; 47: 1004–6.
- Kato T, Shinoda J, Nakayama N, Miwa K, Okumura A, Yano H, et al. Metabolic assessment of gliomas using ¹¹C-methionine, [¹⁸F] fluorodeoxyglucose, and ¹¹C-choline positron-emission tomography. *Am J Neuroradiol* 2008; 29: 1176–82.
- Kinno R, Kawamura M, Shioda S, Sakai KL. Neural correlates of non-canonical syntactic processing revealed by a picture-sentence matching task. *Hum Brain Mapp* 2008; 29: 1015–27.
- Kinno R, Muragaki Y, Hori T, Maruyama T, Kawamura M, Sakai KL. Agrammatic comprehension caused by a glioma in the left frontal cortex. *Brain Lang* 2009; 110: 71–80.
- Krainik A, Lehéry S, Duffau H, Capelle L, Chainay H, Cornu P, et al. Postoperative speech disorder after medial frontal surgery: role of the supplementary motor area. *Neurology* 2003; 60: 587–94.
- Küper M, Timmann D. Cerebellar mutism. *Brain Lang* 2013; 127: 327–33.
- Loui P, Li HC, Schlaug G. White matter integrity in right hemisphere predicts pitch-related grammar learning. *Neuroimage* 2011; 55: 500–7.
- Mandonnet E, Delattre J-Y, Tanguy M-L, Swanson KR, Carpentier AF, Duffau H, et al. Continuous growth of mean tumor diameter in a subset of grade II gliomas. *Ann Neurol* 2003; 53: 524–8.
- Mariën P, De Smet HJ, Wijgerde E, Verhoeven J, Crols R, De Deyn PP. Posterior fossa syndrome in adults: a new case and comprehensive survey of the literature. *Cortex* 2013; 49: 284–300.
- Menn L, Obler LK. Theoretical motivations for the cross-language study of agrammatism. In: Menn L, Obler LK, editors. *Agrammatic aphasia: a cross-language narrative sourcebook*. Amsterdam: John Benjamins Publishing Company, 1990. p. 3–12.
- Meyer M, Friederici AD, von Cramon DY. Neurocognition of auditory sentence comprehension: event related fMRI reveals sensitivity to syntactic violations and task demands. *Cogn Brain Res* 2000; 9: 19–33.
- Musso M, Moro A, Glauche V, Rijntjes M, Reichenbach J, Büchel C, et al. Broca's area and the language instinct. *Nat Neurosci* 2003; 6: 774–81.
- Ojemann JG, Miller JW, Silbergeld DL. Preserved function in brain invaded by tumor. *Neurosurgery* 1996; 39: 253–9.
- Oldfield RC. The assessment and analysis of handedness: the Edinburgh inventory. *Neuropsychologia* 1971; 9: 97–113.
- Price CJ, Friston KJ. Scanning patients with tasks they can perform. *Hum Brain Mapp* 1999; 8: 102–8.
- Pulvermüller F. Agrammatism: behavioral description and neurobiological explanation. *J Cogn Neurosci* 1995; 7: 165–81.
- Rolheiser T, Stamatakis EA, Tyler LK. Dynamic processing in the human language system: synergy between the arcuate fascicle and extreme capsule. *J Neurosci* 2011; 31: 16949–57.
- Sakai KL. Language acquisition and brain development. *Science* 2005; 310: 815–9.
- Sakai KL, Noguchi Y, Takeuchi T, Watanabe E. Selective priming of syntactic processing by event-related transcranial magnetic stimulation of Broca's area. *Neuron* 2002; 35: 1177–82.
- Saur D, Kreher BW, Schnell S, Kümmerer D, Kellmeyer P, Vry M-S, et al. Ventral and dorsal pathways for language. *Proc Natl Acad Sci USA* 2008; 105: 18035–40.
- Saur D, Lange R, Baumgaertner A, Schraknepper V, Willmes K, Rijntjes M, et al. Dynamics of language reorganization after stroke. *Brain* 2006; 129: 1371–84.
- Schwartz MF, Saffran EM, Marin OSM. The word order problem in agrammatism. I. Comprehension. *Brain Lang* 1980; 10: 249–62.
- Seghier ML, Fagan E, Price CJ. Functional subdivisions in the left angular gyrus where the semantic system meets and diverges from the default network. *J Neurosci* 2010; 30: 16809–17.
- Smith SM. The future of fMRI connectivity. *Neuroimage* 2012; 62: 1257–66.
- Stromswold K, Caplan D, Alpert N, Rauch S. Localization of syntactic comprehension by positron emission tomography. *Brain Lang* 1996; 52: 452–73.
- Suzuki K, Sakai KL. An event-related fMRI study of explicit syntactic processing of normal/anomalous sentences in contrast to implicit syntactic processing. *Cereb Cortex* 2003; 13: 517–26.
- Thiel A, Schumacher B, Wienhard K, Gairing S, Kracht LW, Wagner R, et al. Direct demonstration of transcallosal disinhibition in language networks. *J Cereb Blood Flow Metab* 2006; 26: 1122–7.

- Ulmer JL, Hacein-Bey L, Mathews VP, Mueller WM, DeYoe EA, Prost RW, et al. Lesion-induced pseudo-dominance at functional magnetic resonance imaging: implications for preoperative assessments. *Neurosurgery* 2004; 55: 569–81.
- Wilson SM, Dronkers NF, Ogar JM, Jang J, Growdon ME, Agosta F, et al. Neural correlates of syntactic processing in the nonfluent variant of primary progressive aphasia. *J Neurosci* 2010; 30: 16845–54.
- Wilson SM, Galantucci S, Tartaglia MC, Rising K, Patterson DK, Henry ML, et al. Syntactic processing depends on dorsal language tracts. *Neuron* 2011; 72: 397–403.
- Wong FCK, Chandrasekaran B, Garibaldi K, Wong PCM. White matter anisotropy in the ventral language pathway predicts sound-to-word learning success. *J Neurosci* 2011; 31: 8780–5.

Supplementary material

Differential reorganization of three syntax-related networks induced by a left frontal glioma

Ryuta Kinno, Shinri Ohta, Yoshihiro Muragaki, Takashi Maruyama, and Kuniyoshi L. Sakai

Contents:

Supplementary Table 1	2
Supplementary Table 2	3
Supplementary Table 3	4
Supplementary Table 4	5
Supplementary materials and methods	6
Supplementary references	16

Supplementary Table 1 Activation of the syntax-related regions in normal participants ($n = 14$) (Kinno *et al.*, 2008)

Brain region	BA	Side	x	y	z	Z
Two-argument – Control						
LPMC	6/8	L	-45	9	33	5.3
		R	42	6	36	4.3
F3op/F3t	44/45	L	-48	27	15	3.9
		R	48	15	36	3.9
F3t	45	L	-54	30	9	3.9
F3O	47	L	-45	45	-3	3.4
		R	33	21	3	4.6
pre-SMA	6/8	M	9	18	24	5.1
pSTG/MTG	22/21	L	-54	-54	3	5.4
		R	57	-54	9	4.3
pMTG/ITG	37/19	L	-42	-78	-12	4.5
IPS	7/39/40	L	-27	-72	45	5.0
		R	33	-72	45	4.1
AG/SMG	39/40	L	-36	-57	39	4.1
		R	39	-63	45	4.6
Precuneus		M	0	-75	45	5.0
One-argument – Control						
LPMC	6/8	L	-39	0	45	5.1
		R	42	3	36	3.6
pSTG/MTG	22/21	L	-63	-48	9	5.5
		R	54	-63	6	4.3
IPS	7/39/40	L	-24	-78	33	4.2
Two-argument – One-argument						
LPMC	6/8	L	-39	3	33	5.0
F3op/F3t	44/45	L	-45	15	27	4.5
F3t	45	L	-51	39	12	3.1
F3O	47	L	-51	21	-6	3.5
pSTG/MTG	22/21	L	-57	-51	6	5.1
pMTG/ITG	37/19	L	-51	-69	-6	4.1

Stereotactic coordinates (x, y, z) in the Montreal Neurological Institute space are shown for each activation peak of Z values. The threshold was set at corrected $P < 0.05$ for the cluster level.

AG/SMG = angular gyrus/supramarginal gyrus; BA = Brodmann's area; F3O = orbital part of the F3; F3op/F3t = opercular/triangular parts of the F3; F3t = triangular part of the F3; IPS = intraparietal sulcus; L = left; M = medial; pMTG/ITG = posterior middle/inferior temporal gyri; pre-SMA = pre-supplementary motor area; pSTG/MTG = posterior superior/middle temporal gyri; R = right.

Supplementary Table 2 Activation of the syntax-related regions in the patient groups and normal participants ($n = 7$)

Brain region	BA	Side	x	y	z	Z
Analysis of covariance with two factors (group \times condition)						
Main effect of group						
F3op/F3t	44/45	L	-51	15	15	4.0
F3O	47	L	-39	21	-3	3.2
Interaction of group by condition						
LPMC	6/8	L	-42	3	48	5.4
F3op/F3t	44/45	L	-54	15	15	4.6
F3O	47	L	-39	21	-3	4.9
pSTG/MTG	22/21	L	-54	-45	3	4.2
Two-argument – Control						
Normal group						
LPMC	6/8	L	-42	-6	42	4.0
		R	48	9	42	4.2
F3op/F3t	44/45	L	-45	21	24	3.4
F3t	45	L	-51	33	3	3.0
F3O	47	L	-39	18	-3	3.2
pre-SMA	6/8	M	6	24	48	3.8
pSTG/MTG	22/21	L	-54	-48	3	3.5
		R	51	-57	9	3.2
pMTG/ITG	37/19	L	-45	-69	-9	4.1
IPS	7/39/40	L	-38	-54	51	4.1

The threshold was set at corrected $P < 0.05$ for the cluster level.

BA = Brodmann's area; F3O = orbital part of the F3; F3op/F3t = opercular/triangular parts of the F3; F3t = triangular part of the F3; IPS = intraparietal sulcus; L = left; M = medial; pMTG/ITG = posterior middle/inferior temporal gyri; pre-SMA = pre-supplementary motor area; pSTG/MTG = posterior superior/middle temporal gyri; R = right.

Supplementary Table 3 Regions identified by Two-argument – One-argument for each group

Brain region	BA	Side	x	y	z	Z
Normal group						
LPMC	6/8	L	-48	3	42	3.9
F3op/F3t	44/45	L	-45	18	27	3.3
F3t	45	L	-48	33	6	4.3
F3O	47	L	-36	15	-6	2.8
pSTG/MTG	22/21	L	-57	-48	0	3.4
pMTG/ITG	37/19	L	-45	-69	0	4.4
LPMC group						
LPMC	6/8	L	-39	6	48	3.4
		R	30	3	45	3.3
F3op/F3t	44/45	L	-57	18	24	3.1
		R	33	18	24	3.8
F3t	45	L	-57	24	15	4.5
F3O	47	L	-36	27	-12	3.6
pre-SMA	6/8	M	9	24	51	3.2
pSTG/MTG	22/21	L	-51	-39	3	4.2
		R	60	-57	3	2.8
pMTG/ITG	37/19	L	-57	-60	0	3.1
IPS	7/39/40	L	-21	-72	51	4.0
F3 group						
None						
Other group						
LPMC	6/8	L	-48	6	42	4.2
F3op/F3t	44/45	L	-39	18	27	4.5
F3t	45	L	-39	39	6	3.6
F3O	47	L	-39	33	-3	5.2
pSTG/MTG	22/21	L	-57	-48	0	3.6
pMTG/ITG	37/19	L	-51	-75	3	3.0

The threshold was set at corrected $P < 0.05$ for the cluster level.

BA = Brodmann's area; F3O = orbital part of the F3; F3op/F3t = opercular/triangular parts of the F3; F3t = triangular part of the F3; IPS = intraparietal sulcus; L = left; M = medial; pMTG/ITG = posterior middle/inferior temporal gyri; pre-SMA = pre-supplementary motor area; pSTG/MTG = posterior superior/middle temporal gyri; R = right.

Supplementary Table 4 Regions identified by Two-argument – One-argument separately for correct and incorrect responses

Brain region	BA	Side	Correct				Incorrect			
			x	y	z	Z	x	y	z	Z
Normal group										
LPMC	6/8	L	-51	9	42	3.1				
F3op/F3t	44/45	L	-39	18	24	3.6				
F3t	45	L	-42	39	3	4.1				
F3O	47	L	-36	15	-3	2.8				
pSTG/MTG	22/21	L	-54	-39	0	3.7				
pMTG/ITG	37/19	L	-48	-69	3	3.2				
F3 group										
LPMC	6/8	L	-45	9	39	3.9	-42	6	39	3.0
AG	39	L	-33	-60	18	3.8	-33	-66	21	3.1
LG	18	M	-3	-69	6	3.3	0	-75	0	3.0
			9	-87	3	3.5				
cerebellar nuclei		M	-3	-51	-27	4.3	0	-54	-30	4.2

The threshold was set at corrected $P < 0.05$ for the cluster level. In the Normal group, there was no significant activation for incorrect responses in any regions. In contrast, the F3 group showed an exact correspondence between the activated regions for correct and incorrect responses.

AG = angular gyrus; BA = Brodmann's area; F3O = orbital part of the F3; F3op/F3t = opercular/triangular parts of the F3; F3t = triangular part of the F3; L = left; LG = lingual gyrus; M = medial; pMTG/ITG = posterior middle/inferior temporal gyri; pre-SMA = pre-supplementary motor area; pSTG/MTG = posterior superior/middle temporal gyri.

Supplementary materials and methods

Here, we provided a full description of the experimental conditions and the procedures used to acquire the data presented.

Participants

We tested 21 patients, who were native Japanese speakers newly diagnosed as having a left frontal glioma (Table 1). The patients preoperatively performed a picture-sentence matching task (Fig. 1A), and underwent functional MRI scans in an event-related design. The patients were divided into three groups based on the individual tumor locations in the normalized brain (Fig. 1B): patients with a glioma in the left LPMC (LPMC group, $n = 7$); patients with a glioma in the opercular/triangular parts of the left F3 (F3 group, $n = 7$); and patients with a glioma in the other left frontal regions (Other group, $n = 7$). The categorization criterion of each group was whether or not the glioma of a patient overlapped, at least partially on a voxel-by-voxel basis, with functionally identified regions in our previous study (Kinno *et al.*, 2008): the left LPMC shown in Figure 3 of that paper, and the opercular/triangular parts of the left F3 shown in Figure 4 of that paper.

The patients reported here underwent surgery at the Department of Neurosurgery, Tokyo Women's Medical University, after behavioral and functional MRI assessment at the University of Tokyo, Komaba. The following conditions comprised the criteria for inclusion of 21 patients in the present study (Table 1): (i) right-handedness, (ii) no deficits in verbal/written communication or other cognitive abilities reported by the patients or physicians, (iii) no history of neurological or psychiatric disorders other than glioma and seizures, (iv) freedom from seizures with or without antiepileptic drugs, (v) no medical problems related to MRI acquisition, and (vi) completion of at least three functional MRI runs without significant head movement. The types of antiepileptic drugs used were carbamazepine (400 mg/day), gabapentin (600 mg/day), phenobarbital (90-120 mg/day), phenytoin (200-300 mg/day), valproate acid (800-1200 mg/day), and zonisamide (200 mg/day). From our previous study (Kinno *et al.*, 2009), we included seven patients who were scanned with the same functional MRI protocol as used in the present study.

The laterality quotient of handedness was determined by the Edinburgh handedness inventory (Oldfield, 1971). The verbal/nonverbal intelligence quotient was

assessed with the Japanese version of the Wechsler Adult Intelligence Scale-III (1997, 2006; Harcourt Assessment Inc., San Antonio, Texas, USA). Hemispheric dominance was determined by amytal testing, in which the patient counted aloud to a certain number with both hands raised, after an injection of amytal. As soon as contralateral hemiplegia occurred, a picture naming task was performed to examine any speech arrest. The tumor type and grade were postoperatively and pathologically diagnosed by the World Health Organization Classification of Tumors of the Nervous System (2000).

In the present study, we recruited seven normal age-matched participants for functional MRI experiments [Normal group; five males and two females, aged 25-43 years, 31 ± 5.9 (mean \pm standard deviation)]. Eleven normal age-matched participants (ten males and one female, aged 19-40 years, 29 ± 6.0) were also tested in the diffusion tensor imaging studies. The four normal participants that took part in the functional MRI studies were a subset of the diffusion tensor imaging participants. Written informed consent was obtained from each participant after the nature and possible consequences of the studies were explained. Approval for the experiments was obtained from the institutional review board of the University of Tokyo, Komaba, as well as of the Tokyo Women's Medical University.

Lesion analyses

The glioma was first identified on the normalized T1-weighted structural image, and the glioma boundary was semi-automatically determined using the 3D Fill tool in MRICroN software (<http://www.mccauslandcenter.sc.edu/mricro/mricron/>), which generated a contiguous cluster of voxels defined by the intensity of the glioma itself. The boundary of each lesion, including brain edemas and abnormalities of perfusion, was confirmed with T2-weighted MR images taken at the Department of Neurosurgery, Tokyo Women's Medical University. The absence of any skip lesions distant from a tumor was confirmed with ^{11}C -methionine, [^{18}F] fluorodeoxyglucose, and ^{11}C -choline PET data (resolution = $4.8 \times 4.8 \times 4.25 \text{ mm}^3$) taken at the Chubu Medical Center for Prolonged Traumatic Brain Dysfunction (Minokamo City, Gifu, Japan). Lesion overlap maps (Fig. 1B), as well as each patient's activated regions that were transformed back to the individual brains, were shown using MRICroN software.

Stimuli

Each visual stimulus consisted of a picture with head symbols (\circ , \square , or Δ) at the top, and of an always grammatical sentence at the bottom (Fig. 1A). For each stimulus, we chose two different head symbols. The sentences describing actions were written using a combination of the hiragana and kanji writing systems. In Japanese syntax, the grammatical relations (“subject, direct object, or indirect object” in linguistic terms) are first marked by grammatical particles (nominative, dative, or accusative), which in turn allow the assignment of semantic roles (“agent, experiencer, or patient” in linguistic terms, i.e., an agent who initiates the action, and an experiencer/patient who is affected by it), whereas passiveness is also marked in the verb morphology (*-areru*). We used four kinds of grammatical particles, which represent the syntactic information in Japanese: *-ga*, a nominative case marker; *-ni*, a dative case marker; *-o*, an accusative case marker; and *-to*, a coordinator (*and*). Two sets of Japanese verbs (six transitive verbs: *pull*, *push*, *scold*, *kick*, *hit*, and *call*; and six intransitive verbs: *lie*, *stand*, *walk*, *run*, *tumble*, and *cry*) were used, each of which, including the passive forms, had either four or five syllables. Note that the verb “*call*” is used only as a transitive verb in Japanese. There was no significant difference in frequency between the two sets of verbs ($t(10) = 0.7$, $P = 0.5$), according to the Japanese lexical database (“Nihongo-no Goitokusei” (Lexical Properties of Japanese), Nippon Telegraph and Telephone Corporation Communication Science Laboratories, Tokyo, Japan, 2003). The numbers of syllables and letters were strictly controlled among all conditions.

Using the same task, we tested two types of conditions with different sets of stimuli: Two-argument and One-argument conditions. Under the Two-argument conditions with an identical picture set, we tested three different sentence types: active, passive, and scrambled sentences. Scrambled sentences are perfectly normal, not only in Japanese but in German, Finnish, and other languages. Under the Two-argument conditions, each sentence ended with a transitive verb, and had two arguments (phrases associated with the predicate) with different grammatical relations and semantic roles. More specifically, the active, passive, and scrambled sentences corresponded to “subject and direct object” (agent and patient), “subject and indirect object” (experiencer and agent), and “direct object and subject” (patient and agent) types, respectively.

Under the One-argument condition, each sentence ended with an intransitive verb, and corresponded to a “double subjects” (double agents) type, which did not

involve two-argument relationships. A linguistically meaningful contrast is thus “Two-argument – One-argument,” where we averaged together activations under the Active, Passive, and Scrambled sentence conditions. This contrast mainly involved syntactic processes, together with minimal semantic processes of semantic role assignment (experiencer/patient) and lexico-semantics (verb types), whereas general cognitive processes were well controlled. Under the Two-argument conditions, the number of lines used in each picture except the head symbols was 14 ± 2.4 , whereas under the One-argument condition, equally complex pictures (number of lines, 14 ± 2.5) were used. Under both conditions, half of the pictures depicted actions occurring from left to right, and the other half depicted actions occurring from right to left (see Fig. 1A); head symbols were also counterbalanced for both sides. These pictures further excluded the involvement of pragmatic information about word use (e.g., “*An officer chases a thief*” is more acceptable than “*A thief chases an officer*”). There were 48 different stimuli (i.e., different combinations between pictures and sentences) for each of the Active, Passive, and Scrambled sentence conditions, as well as for the One-argument condition.

All stimuli were presented visually in yellow against a dark background (Fig. 1A). Each stimulus was presented for 5800 ms (intratrial interval) followed by a 200 ms blank interval. To minimize the effect of general memory demands, a whole sentence of a minimal length (i.e., two noun phrases and a verb) was visually presented for an ample time for the patients to respond (see Table 2 for the reaction times). The stimuli are thus more advantageous than sequentially presented stimuli that involve memorization. For fixation, a red cross was also shown at the center of the screen to initiate eye movements from the same fixed position, and the participants were instructed to return their eyes to this position after the response. The stimulus presentation and collection of behavioral data (error rates and reaction times) were controlled using the LabVIEW software and interface (National Instruments, Austin, Texas, USA). The participants wore earplugs and an eyeglass-like MRI-compatible display (resolution, 800×600 ; VisuaStim XGA, Resonance Technology Inc., Northridge, California, USA).

Task

In the picture-sentence matching task, the participants read a sentence covertly and judged whether or not the action depicted in a picture matched the meaning of the

sentence. They responded by pressing one of two buttons in a row (right for a matched pair, and left for a mismatched pair). Under the Two-argument conditions, all mismatched sentences were made by exchanging two symbols in the original sentences, e.g., “○ pulls Δ” instead of “Δ pulls ○”. Under the One-argument condition, symbol-mismatched and action-mismatched sentences were presented equally often, requiring the sentences to be read completely. The participants underwent short practice sessions before task sessions to become fully familiarized with this task.

Using the same stimulus sets of pictures and letters presented under both Two-argument and One-argument conditions, we tested a Control task, in which the participants judged whether or not two head symbols in the picture matched those at the bottom, irrespective of their order (Fig. 1A). The letters in hiragana were jumbled without changing the head symbols and kanji, so that the letter string prevented even basic word recognition. General cognitive factors such as visual perception of the stimuli, matching, response selection, and motor responses were controlled by the Control task, and obviously by the One-argument condition as well.

A single run of the task sessions (306 s) contained 24 “test events” of the picture-sentence matching task (six times each for the Active, Passive, and Scrambled sentences, as well as for One-argument), with variable inter-trial intervals of one (6 s) or two (12 s) Control tasks. The order of the test events was pseudorandomized without repetition of the same condition to prevent any condition-specific strategy. A single run contained 27 trials of the Control task.

Eight runs were tested per one participant in a day. Considering the medical conditions of patients, we limited the MR scanning time to one hour with inter-task intervals of 5 min, restricting the number of in-scanner runs. All patients underwent three or four in-scanner runs, and they performed out-scanner runs to make up eight runs. Normal participants were also tested under the same conditions, i.e., four in-scanner and four out-scanner runs. We analyzed behavioral data for the eight runs.

MRI data acquisition

The functional MRI scans were conducted on a 1.5 T scanner (Stratis II, Premium; Hitachi Medical Corporation, Tokyo, Japan). We scanned 26 axial slices of 3-mm thickness with a 1-mm gap, covering from –40 to 63 mm from the anterior to posterior commissure line in the vertical direction, using an echo-planar imaging sequence (repetition time = 3 s, echo time = 50.5 ms, flip angle = 90°, field of view = 192 × 192

mm², resolution = 3 × 3 mm²). In a single scanning run, we obtained 102 volumes following three dummy images, which allowed for the rise of the MR signals. After completion of the functional MRI sessions, high-resolution T1-weighted images of the whole brain (192 axial slices, 0.75 × 0.75 × 1 mm³) were acquired from all participants with a radio frequency spoiled steady-state acquisition with a rewind gradient echo sequence (repetition time = 30 ms, echo time = 8 ms, flip angle = 60°, field of view = 192 × 192 mm²).

The diffusion tensor imaging scans were conducted on a 3.0 T scanner equipped with an 8-channel phased-array head coil (Signa HDxt; GE Healthcare, Milwaukee, Wisconsin, USA). We scanned 50 axial slices of 3-mm thickness without gaps, covering from –60 to 90 mm from the anterior to posterior commissure line in the vertical direction, using a diffusion-weighted spin-echo echo-planar imaging sequence (*b*-value = 1000 s/mm², repetition time = 15 s, echo time = 86.6 ms, field of view = 256 × 256 mm², resolution = 2 × 2 mm², number of excitations = 2). A single image without diffusion-weighting (*b*₀) was initially acquired, and then diffusion-weighting was isotropically distributed along 60 diffusion-encoding gradient directions. After completion of the diffusion tensor imaging sessions, high-resolution T1-weighted images of the whole brain (192 axial slices, 1 × 1 × 1 mm³) were acquired from all participants with a fast spoiled gradient recalled acquisition in the steady state sequence (repetition time = 10.4 ms, echo time = 4.38 ms, flip angle = 25°, field of view = 256 × 256 mm²).

Functional MRI data analyses

Both group and single-subject analyses were performed in a standard manner using SPM8 statistical parametric mapping software (Wellcome Trust Centre for Neuroimaging, <http://www.fil.ion.ucl.ac.uk/spm/>) (Friston *et al.*, 1995), implemented on MATLAB software (MathWorks, Natick, Massachusetts, USA). The acquisition timing of each slice was corrected using the middle slice (the thirteenth slice chronologically) as a reference for the echo-planar imaging data. We realigned the time-series data to the first volume in each run, and removed runs that included data with a translation of > 2 mm in any of the three directions and with a rotation of > 1.4° around any of the three axes; these thresholds of head movement were empirically determined from our previous studies (Hashimoto and Sakai, 2002; Suzuki and Sakai, 2003; Kinno *et al.*, 2008). For this reason, a single run was removed from three normal participants, two

patients in the LPMC group, three patients in the F3 group, and two patients in the Other group, which was about 10% of all time points.

Each participant's T1-weighted structural image was coregistered to the mean functional image generated during realignment. The coregistered structural image was spatially normalized to the standard brain space as defined by the Montreal Neurological Institute using the "unified segmentation" algorithm with medium regularization, which is a generative model that combines tissue segmentation (excluding "other" tissues like a lesion, etc.), bias correction, and spatial normalization (Ashburner and Friston, 2005). All of the normalized structural images were visually inspected and compared with the standard brain for the absence of any further deformation. A previous study has suggested that the unified models provide better and more reliable matching for brain images with focal lesions (Crinion *et al.*, 2007). After spatial normalization, the resultant deformation field was applied to the realigned echo-planar imaging data in each run, which was resampled every 3 mm using seventh-degree B-spline interpolation. All normalized functional images were then smoothed by using an isotropic Gaussian kernel of 9 mm full-width at half maximum. Low-frequency noise was removed by high-pass filtering at 1/128 Hz.

In a first-level analysis (i.e., fixed-effects analysis), each participant's hemodynamic responses induced by the trials were modeled with a boxcar function with a duration of 6 s from the onset of each stimulus, and the boxcar function was convolved with a hemodynamic response function. The functional data for trials with correct and incorrect responses in the picture-sentence matching task were separately modeled. To minimize the effect of head movement, the six realignment parameters obtained from preprocessing were included as a nuisance factor in a general linear model. The images of the Active, Passive, and Scrambled sentence conditions, as well as those of the Two-argument, One-argument, and Control, were then generated in the general linear model for each participant, and used for intersubject comparisons in a second-level analysis (i.e., random-effects analysis).

To discount any general effects associated with performance differences among the participants, individual error rates averaged among the Two-argument conditions, or those of the One-argument condition for the One-argument – Control contrast, were entered as a nuisance factor in a second-level analysis. Note that error rates were more sensitive among the Two-argument conditions than reaction times (see Table 2). The results of paired *t*-tests (Two-argument – Control, One-argument –

Control, or Two-argument – One-argument) were thresholded at $P < 0.005$ for the voxel level, and at corrected $P < 0.05$ for the cluster level, with topological false discovery rate correction across the whole brain (Chumbley and Friston, 2009).

An analysis of covariance with F -test was performed with two factors [group (LPMC, F3, Other) \times condition (Active, Passive, Scrambled)] using the toolbox “Non-Stationary Cluster Extent Correction for SPM” (<http://fmri.wfubmc.edu/cms/software#NS>), the results of which were thresholded at $P < 0.005$ for the voxel level, and at corrected $P < 0.05$ for the cluster level, with family-wise error correction across the whole brain. Individual error rates were entered as a nuisance factor for each of the Active, Passive, and Scrambled sentence conditions. For the anatomical identification of activated regions, we basically used the Anatomical Automatic Labeling method (Tzourio-Mazoyer *et al.*, 2002). For each region of interest, the mean percent signal changes were extracted from the local maximum using the MarsBaR-toolbox (<http://marsbar.sourceforge.net/>).

Functional connectivity analyses

By using functional MRI data, functional connectivity among multiple regions was assessed by a partial correlation method for the time-series data of the Normal group. Using MarsBaR-toolbox, the time-series data were first averaged within a sphere of 6-mm radius centered at the local maximum of each region. To discount the global differences of signal changes among the runs, the time-series were normalized for each run. From each of the time-series of two regions in question, we regressed out all the other nodes, before estimating the correlation between the two. For each participant, partial correlation coefficients for each pair of regions were calculated using MATLAB, and they were averaged among all participants to create a partial correlation matrix (Fig. 7C).

We tested whether the non-diagonal correlations *within* individual networks were significantly greater than those *between* any of two networks. Because the partial correlation coefficients were not normally distributed, we adopted the randomization analyses (Nichols and Holmes, 2002); we randomized the labels of the regions, reordered their corresponding columns, computed partial correlation coefficients for each pair of regions, and then averaged them among all participants. For each randomized partial correlation matrix, we averaged the non-diagonal correlations within individual networks, as well as those between two networks, and subtracted the

latter from the former. Repeating these steps 10,000 times, we estimated the *P*-value for the significance of an observed difference in partial correlations.

Diffusion tensor imaging data analyses

Data analyses of diffusion tensor imaging were performed using FSL (Oxford Centre for FMRIB Software Library 4.1.7; <http://fsl.fmrib.ox.ac.uk/fsl/fslwiki/>) and FDT (FMRIB's Diffusion Toolbox 2.0) (Smith *et al.*, 2004). Diffusion-weighted images were first resliced to isotropic voxels of 1 mm³, and then eddy current distortions and motion artifacts were corrected using affine registration to the b0 image. We then extracted the brain shape from the b0 image, and created the binary mask image (i.e., zero for the outside of the brain) for each participant. Markov Chain Monte Carlo sampling was performed to build up distributions on diffusion parameters at each voxel, which allowed for estimation of the most probable pathway by Bayesian estimation (number of fibers modeled per voxel = 2) (Behrens *et al.*, 2007). The implicit modeling of noise in a probabilistic model made it possible to track the fibers near the grey matter.

By using FLIRT (FMRIB's Linear Image Registration Tool) on FSL, the b0 image was first coregistered to the individual T1-weighted image for each participant, and the T1-weighted image was spatially normalized to the Montreal Neurological Institute space by using both affine and nonlinear transformations with FLIRT and FNIRT (FMRIB's Nonlinear Image Registration Tool). With the transformation matrices and estimated deformation fields, the coordinates of each region were transformed back to the individual b0 images, and a sphere of 6-mm radius centered at the transformed coordinates was defined as a seed mask for the probabilistic tractography. All fiber tracking was conducted in an individual diffusion tensor imaging space.

To find the connections between two regions of interest, we set two seed masks and retained only those tracts that passed through both seed masks. Probabilistic fiber tracking was initiated from all voxels within the seed masks to generate 10,000 streamline samples, with a step length of 0.5 mm, a maximum number of steps of 2,000, a curvature threshold of 0.2 ($\pm 78.5^\circ$), and a loopcheck option. For the pathway of the opercular/triangular parts of the right F3 & right posterior superior/middle temporal gyri (“&” denotes a pair of seed masks), as well as that of the left angular gyrus & lingual gyrus, an exclusion mask of the corpus callosum and fornix was applied; for the pathway of the opercular/triangular parts of the right F3 & pre-supplementary motor area, an exclusion mask of the midbrain was applied.

In the connectivity distributions obtained, each voxel value represented the total number of the streamline samples passing through that voxel. The connectivity probability maps were then created for each participant by dividing the connectivity distributions with a sum of the waytotal values, i.e., the total number of generated tracts from one seed mask that reached the other seed mask. This normalization approach allowed for a comparison of the connectivity probability values across participants; note that the pattern of connectivity did not change by this scaling. To remove any spurious connections, the pathways in individual participants were thresholded to include only voxels that had at least 1% connectivity probability values (Flöel *et al.*, 2009). The thresholded pathways in each participant were spatially normalized, and then binarized using “fslmaths” on FSL. The binarized pathways were overlaid across participants to produce a population probability map for each pathway, in which the voxel values represent the number of participants with a pathway through that voxel. The population probability map with thresholding (at least five out of 11 participants) was smoothed and presented using MRICroN software.

Supplementary References

- Ashburner J, Friston KJ. Unified segmentation. *Neuroimage* 2005; 26: 839-51.
- Behrens TEJ, Berg HJ, Jbabdi S, Rushworth MFS, Woolrich MW. Probabilistic diffusion tractography with multiple fibre orientations: What can we gain? *Neuroimage* 2007; 34: 144-55.
- Chumbley JR, Friston KJ. False discovery rate revisited: FDR and topological inference using Gaussian random fields. *Neuroimage* 2009; 44: 62-70.
- Crinion J, Ashburner J, Leff A, Brett M, Price C, Friston K. Spatial normalization of lesioned brains: Performance evaluation and impact on fMRI analyses. *Neuroimage* 2007; 37: 866-75.
- Flöel A, de Vries MH, Scholz J, Breitenstein C, Johansen-Berg H. White matter integrity in the vicinity of Broca's area predicts grammar learning success. *Neuroimage* 2009; 47: 1974-81.
- Friston KJ, Holmes AP, Worsley KJ, Poline J-P, Frith CD, Frackowiak RSJ. Statistical parametric maps in functional imaging: A general linear approach. *Hum Brain Mapp* 1995; 2: 189-210.
- Hashimoto R, Sakai KL. Specialization in the left prefrontal cortex for sentence comprehension. *Neuron* 2002; 35: 589-97.
- Kinno R, Kawamura M, Shioda S, Sakai KL. Neural correlates of noncanonical syntactic processing revealed by a picture-sentence matching task. *Hum Brain Mapp* 2008; 29: 1015-27.
- Kinno R, Muragaki Y, Hori T, Maruyama T, Kawamura M, Sakai KL. Agrammatic comprehension caused by a glioma in the left frontal cortex. *Brain Lang* 2009; 110: 71-80.
- Nichols TE, Holmes AP. Nonparametric permutation tests for functional neuroimaging: A primer with examples. *Hum Brain Mapp* 2002; 15: 1-25.
- Oldfield RC. The assessment and analysis of handedness: The Edinburgh inventory. *Neuropsychologia* 1971; 9: 97-113.
- Smith SM, Jenkinson M, Woolrich MW, Beckmann CF, Behrens TEJ, Johansen-Berg H et al. Advances in functional and structural MR image analysis and implementation as FSL. *Neuroimage* 2004; 23: S208-S219.
- Suzuki K, Sakai KL. An event-related fMRI study of explicit syntactic processing of normal/anomalous sentences in contrast to implicit syntactic processing. *Cereb Cortex* 2003; 13: 517-26.
- Tzourio-Mazoyer N, Landeau B, Papathanassiou D, Crivello F, Etard O, Delcroix N et al. Automated anatomical labeling of activations in SPM using a macroscopic anatomical parcellation of the MNI MRI single-subject brain. *Neuroimage* 2002; 15: 273-89.